High-Intensity Interval Training Remodels the Proteome and Acetylome of Human Skeletal Muscle

Hostrup M[1+*], Lemminger AK[1+], Stocks B[2+], Gonzalez-Franquesa A[2], Larsen JK[2], Thomassen M[1], Weinert BT[3], Bangsbo J[1], & Deshmukh AS[2,4*]

[1]Section of Integrative Physiology, Department of Nutrition, Exercise and Sports, University of Copenhagen, Copenhagen, Denmark

[2]Novo Nordisk Foundation Center for Basic Metabolic Research, Faculty of Health and Medical Sciences, University of Copenhagen, Copenhagen, Denmark

[3]The Novo Nordisk Foundation Center for Biosustainability, Technical University of Denmark, Copenhagen, Denmark.

[4]The Novo Nordisk Foundation Center for Protein Research, Clinical Proteomics, Faculty of Health and Medical Sciences, University of Copenhagen, Copenhagen, Denmark.

[+]Joint first-authors

***Corresponding authors:**

Atul S Deshmukh (Lead contact)

Novo Nordisk Foundation Center for Basic Metabolic Research, Faculty of Health and Medical Sciences, University of Copenhagen, Blegdamsvej 3B, DK2200, Copenhagen, Denmark

Phone: +45 35 32 53 13; e-mail: atul.deshmukh@sund.ku.dk

Morten Hostrup

Section of Integrative Physiology, Department of Nutrition, Exercise and Sports, University of Copenhagen, 13, Universitetsparken, DK 2100, Denmark

Phone: +45 24 47 47 85; e-mail: mhostrup@nexs.ku.dk

Abstract

Exercise is an effective strategy in the prevention and treatment of metabolic diseases. Alterations in the skeletal muscle proteome, including post-translational modifications, regulate its metabolic adaptations to exercise. Here, we examined the effect of high-intensity interval training (HIIT) on the proteome and acetylome of human skeletal muscle, revealing the response of 3168 proteins and 1263 lysine acetyl-sites on 464 acetylated proteins. We identified global protein adaptations to exercise training involved in metabolism, excitation-contraction coupling, and myofibrillar calcium sensitivity. Furthermore, HIIT increased the acetylation of mitochondrial proteins, particularly those of complex V, likely via non-enzymatic mechanisms. We also highlight the regulation of exercise-responsive histone acetyl-sites. These data demonstrate the plasticity of the skeletal muscle proteome and acetylome, providing insight into the regulation of contractile, metabolic and transcriptional processes within skeletal muscle. Herein, we provide a substantial hypothesis-generating resource to stimulate further mechanistic research investigating how exercise improves metabolic health.

Introduction

Exercise training is the most effective means to improve cardiovascular fitness and metabolic health, both being predominant determinants of life expectancy and all-cause mortality[1]. Alterations to the proteome of skeletal muscle underpin its adaptations to exercise training, including glucose and fatty acid metabolism, insulin sensitivity, mitochondrial respiration, immune function and excitation-contraction coupling[2-8]. Furthermore, proteome-wide post-translational modifications play an important role in regulating metabolism via modulating signaling, protein stability and enzyme activity[9,10], and are sensitive to exercise stimuli[11-13].

The application of mass-spectrometry-based proteomics has vastly expanded the catalog of post-translationally modified proteins, including acetylated proteins, and in doing so has revealed novel insights into both histone and non-histone acetylation[14-17]. Nevertheless, the understanding of the acetylome in human skeletal muscle is still incomplete and remains to be studied in response to exercise training. Numerous cellular processes are regulated by protein acetylation, including transcription, metabolism, apoptosis, growth and muscle contraction among others[16]. Lysine acetylation is an evolutionarily conserved post-translational modification, whereby lysine acetyltransferases catalyze the transfer of an acetyl group from acetyl-CoA to the ε-amino acid side chain of lysine and deacetylases remove acetyl groups from lysine residues. Alternatively, acetyl groups can be non-enzymatically transferred to lysine from acetyl-CoA. In human *vastus lateralis* muscle biopsies from male athletes, 941 acetylated proteins containing 2811 lysine acetylation sites have been identified[18]. Mitochondria were the cellular component of human skeletal muscle exhibiting the greatest proportion of acetylated proteins[18]. Furthermore, the sensitivity of the acetylome to physiological stimuli has been demonstrated in rodents in response to acute fasting and

60 chronic caloric restriction in liver[19-21] as well as acute exercise[12] and high-fat diet[22] in skeletal
61 muscle[12].
62
63 Continual advances in mass spectrometry-based proteomic technologies and approaches are
64 increasing the depth and coverage of proteomic analyses. Nevertheless, proteome and proteome-wide
65 post-translational modification analyses of skeletal muscle tissue remain highly challenging due to a
66 wide dynamic range of protein expression[23]. Single-shot data-dependent acquisition (DDA) analyses
67 are often limited in their protein identifications and are characterized by relatively poor data
68 completeness (i.e. high number of missing values)[24]. However, the relatively recent development of
69 data-independent acquisition (DIA) is helping to vastly reduce the proportion of missing data while
70 simultaneously improving proteome depth in single-shot analyses of complex tissues[25]. Nonetheless,
71 DDA in combination with peptide-level fractionation remains a useful approach to overcome sample
72 complexity, particularly when performing post-translational modification proteomics.
73
74 In this study, untrained men undertook five weeks of high-intensity interval training (HIIT) and *vastus*
75 *lateralis* muscle biopsies were collected before and after HIIT for proteomic and lysine-acetylome
76 analyses. We produced the largest single-shot human skeletal muscle proteome to date and undertook
77 the first investigation of the acetylomic adaptations to exercise training within human skeletal muscle.
78 HIIT remodeled skeletal muscle favoring mitochondrial biogenesis, but induced changes in protein
79 expression indicative of reduced calcium sensitivity. Furthermore, HIIT increased acetylation,
80 particularly of the mitochondria and enzymes of the tricarboxylic acid (TCA) cycle.
81
82 **Results and Discussion**
83 **Physiological adaptations to HIIT**

Eight untrained men (23–38 years of age) completed a HIIT regimen (Fig. 1A) that consisted of five weeks of supervised cycling, performed as 4 – 5 × 4-min intervals at a target heart rate of >90%-max interspersed by 2 mins of active recovery, undertaken three times weekly. Participants were healthy, non-smokers and occasionally active, but otherwise untrained. Characteristics of the participants are presented in Fig. 1B. Participants experienced a 14% and 17% improvement in $\dot{V}O_{2max}$ and incremental peak power output, respectively, during HIIT (Fig. 1B and C; $p < 0.001$), which compares favorably to typical HIIT-induced adaptations[26]. In addition, participants gained an average of 1.0 ± 0.3 kg lean mass during HIIT training, without changes in fat mass (Fig. 1B). The rate of fat oxidation during submaximal cycling (50-150 W) increased following HIIT (Fig. 1D), while no apparent changes were observed for carbohydrate oxidation (Fig. 1E).

HIIT increases mitochondrial respiratory capacity of skeletal muscle

Resting muscle biopsies were collected from the *vastus lateralis* before and three days after the final training session. Mitochondrial respirometry analyses were immediately performed on the freshly excised muscle samples using a substrate-uncoupler-inhibitor titration protocol[27] on a high-resolution O2K respirometer (Oroboros, Innsbruck, Austria). In line with previous findings[28-33], HIIT increased mitochondrial respiration across a range of respiratory states, increasing CI+II coupled respiration by 30% ($p < 0.001$) and electron transport system capacity by 15% ($p = 0.049$) (Fig. 1F). Furthermore, HIIT induced a robust increase in citrate synthase activity by 42% ($p = 0.002$) (Fig. 1G), a validated marker of mitochondrial volume in human skeletal muscle[34].

Elevated mitochondrial respiration is underpinned by increased expression of mitochondrial proteins following HIIT

107 Skeletal muscle biopsy samples were prepared for liquid-chromatography tandem mass spectrometry
108 and measured using single-shot DIA[25] (Fig. 1H). We obtained extensive proteome coverage
109 identifying 3343 proteins (Table S1), the largest human single-shot skeletal muscle proteome to date.
110 After applying a filter of 4 valid values out of the 8 participants in at least one time point, 3168
111 proteins were quantified within skeletal muscle (Table S2). Due to the nature of DIA, few missing
112 values required imputation in each sample (Fig. S1A; mean proteins quantified per sample: 2853 ±
113 33). Good correlation (median correlation: 0.88) between biological replicates (participants at the
114 same time point) was apparent (Fig. S1B). Furthermore, the proteome contained good coverage across
115 multiple cellular compartments (Fig. S1C). Thus, our DIA proteome analysis displayed extensive
116 coverage and data completeness.
117
118 HIIT regulated 126 proteins (permutation-based FDR<0.05). Of these, 102 proteins were upregulated,
119 while 24 were downregulated (Fig. 2A, Table S2). These included the upregulation of classical
120 endurance exercise training-responsive mitochondrial proteins (e.g. cytochrome c oxidase subunit 5b;
121 COX5B & NADH dehydrogenase 1 alpha subcomplex subunit 7; NDUFA7), as well as proteins
122 involved in NAD^+ metabolism (e.g. nicotinamide phosphoribosyltransferase; NAMPT), branched-
123 chain amino acid metabolism (branched-chain alpha-ketoacid dehydrogenase kinase; BCKDK) and
124 ubiquinone biosynthesis (5-demethoxyubiquinone hydroxylase; COQ7), the latter of which we have
125 recently described in exercise-trained mouse skeletal muscle[3] (Fig. 2A). We also identified novel
126 exercise-training regulated proteins, including, but not limited to, glutaminyl-tRNA synthase (QARS)
127 and rab GDP dissociation inhibitor alpha (GDI1). QARS, which catalyzes the glutamate
128 aminoacylation of tRNA and thus plays a central role in translation (Deutscher, 1984), was amongst
129 the most significantly upregulated proteins within the proteome. In addition, GDI1, which inhibits

130 insulin-stimulated glucose uptake by preventing the dissociation of GDP from Rab10[35], was lowered,
131 providing a novel potential mechanism for the insulin-sensitizing effects of exercise training.
132
133 After filtering for differentially regulated proteins, enrichment analysis using Fisher's exact test
134 indicated the predominant regulation of mitochondrial proteins (e.g. GOCC: mitochondrial part and
135 mitochondrial inner membrane) (Fig. 2B, Table S3). Hierarchical clustering analysis on z-scored
136 differentially regulated proteins identified that the mitochondrial terms were enriched within the
137 upregulated proteins (Fig. 2C). Summed protein abundances also demonstrated mitochondrial
138 biogenesis (Fig. 2D), including upregulated protein content of electron transport chain complexes
139 (Fig. 2E and S2), mitochondrially-encoded proteins (Fig. 2F) and proteins containing a mitochondria-
140 targeting transit peptide (Fig. 2G). Thus, the increase in the proteome mirrors the functional increase
141 in mitochondrial respiratory capacity of skeletal muscle after HIIT (Fig. 1F).
142
143 **HIIT regulates proteins involved in skeletal muscle excitation-contraction coupling**
144 We next investigated whether HIIT influenced the fiber-type proportions of skeletal muscle. While
145 HIIT did not change skeletal muscle fiber-type composition in terms of myosin heavy chain isoforms
146 (Fig. 3A) and myosin light chain proteins (Fig. 3B), a coordinated regulation of proteins modulating
147 myosin light chain phosphorylation was identified (Fig. 3C). Expression of myosin light chain kinase
148 2 (MYLK2) decreased concomitantly with a reduction in smoothelin-like protein 1 (SMTNL1), an
149 inhibitor of the myosin phosphatase complex[36] and an increase in myosin phosphatase-targeting
150 subunit 1 (PPP1R12A), the myosin-targeting regulatory subunit of protein phosphatase 1[37] (Fig. 3C).
151 Reduced MYLK2 expression was confirmed by immunoblotting (Fig. S3A). Furthermore, we have
152 previously detected these adaptations in slow- and fast-twitch muscle fibers following moderate-
153 intensity continuous cycling training[2]. Given that phosphorylation of myosin light chains promotes

154 myofibrillar calcium sensitivity[38], the reduction in both MYLK2 and SMTNL1 alongside an increase
155 in PPP1R12A indicates an adaptation towards reduced myosin phosphorylation and lowered calcium
156 sensitivity following exercise training. Indeed, myofibrillar calcium sensitivity decreases following
157 high-intensity sprint training in untrained males, particularly at a low pH representing physiological
158 exercising conditions[39]. Although the functional importance of such adaptations remains elusive,
159 knockdown of Smtnl1 augments exercise training-induced improvements in endurance performance,
160 while sedentary Smtnl1$^{-/-}$ mice display a fiber-type switch mimicking endurance exercise training[36].
161 Although we did not observe any concomitant myosin fiber-type switching (Fig. 3A), the changes
162 observed in proteins regulating myosin phosphorylation following HIIT could result in a right-shift
163 of the Ca^{2+}-force relationship, meaning that a higher myoplasmic calcium concentration would be
164 required for a given force production. This decline in myofibrillar calcium sensitivity may, however,
165 support faster off-kinetics of calcium from troponin-C to be re-sequestered in the sarcoplasmic
166 reticulum. Therefore, the changes observed in proteins regulating myosin phosphorylation following
167 HIIT provide an intriguing mechanism for a HIIT-induced reduction in calcium sensitivity and
168 warrants further attention.
169
170 Providing a further link to the altered calcium handling following HIIT[39], we identified a
171 downregulation of L-type calcium channel subunits, otherwise known as the dihydropyridine receptor
172 (DHPR) (Figs. 3 D and E). DHPR controls the coupling of membrane depolarization and
173 sarcoplasmic reticulum Ca^{2+}-release in skeletal muscle via its interaction with ryanodine receptor 1
174 (RYR1)[40]. Conversely to DHPR, HIIT did not influence the expression of RYR1 (Fig. 3F) or the
175 sarcoplasmic/endoplasmic reticulum calcium ATPases 1-3 (ATP2A1-3 (SERCAs); Fig. S3B). The
176 observation that DHPR abundance declined following HIIT points to a 'slowing' of muscle fibers.
177 Indeed, a period of training can induce rapid changes in the expression of proteins with importance

178 for calcium handling, irrespective of changes in fiber type distribution[41-45]. Fast-twitch fibers have
179 greater sarcoplasmic reticulum volume, faster calcium release and re-uptake kinetics, and a greater
180 content of DHPR than slow-twitch fibers[2,46,47]. Thus, the HIIT-induced reduction of DHPR
181 expression may represent a slowing of muscle fibers independently of their myosin heavy chain
182 expression.
183

184 **Lysine acetylomics of skeletal muscle identifies the predominant acetylation of mitochondrial**
185 **and acetyl-coA metabolic proteins**

186 Skeletal muscle biopsy samples were prepared for lysine acetylomics using a PTMscan Acetyl-Lysine
187 Motif kit (Cell Signaling Technology)[17] and measured via liquid-chromatography tandem mass
188 spectrometry using DDA. Due to limited sample availability from one participant, lysine acetylomics
189 was performed for 7 of the participants. We identified a total of 1990 acetyl-sites on 664 proteins
190 (Table S4). While this is fewer than the 2811 acetyl-sites on 941 proteins identified in the largest
191 human skeletal muscle acetylome to date[18], we identified 1073 acetyl-sites that were not identified in
192 the analysis of Lundby et al (Fig. S4A), thus substantially extending the human skeletal muscle
193 acetylome. After applying a filter of 4 valid values, out of the 7 participants in at least one time point
194 we quantified 1263 acetylated sites on 464 proteins within skeletal muscle (Figs. 1G & 4A, Table
195 S5). Six and 42 acetyl-sites were quantified exclusively in the pre- and post-HIIT samples,
196 respectively. The mean number of acetyl-sites quantified in each sample was 976 (Fig. S4B). Median
197 correlation between biological replicates (between participants at the same time point) was 0.76 (Fig.
198 S4C), indicating greater variation in the human acetylome than the proteome, as would be expected[18].
199 The acetylome also displayed extensive coverage across multiple cellular compartments (Fig. S4D),
200 which largely reflected the abundance distribution of the proteome (Fig. S1C), albeit with a slight
201 relative increase in the mitochondrial identifications. There was considerable overlap with proteins

202 quantified in the proteome, with 421 proteins quantified in both (Fig. 4A). Of the quantified acetylated
203 sites (1263), the majority (1232) were located on these 421 proteins (Fig. 4A). Single acetyl-sites
204 were quantified on the majority of proteins, with a trend for decreasing frequency with additional
205 acetyl-sites (Fig. 4B). However, several proteins were quantified with a large number of acetylation
206 sites (e.g. ≥ 15 acetyl-sites) (Fig. 4B), examples of which include the contractile proteins titin (TTN)
207 and slow-twitch myosin beta (MYH7).
208
209 After summing the median intensities of acetyl peptides from each protein in the pre-HIIT samples,
210 we ranked the abundance of acetylated proteins within skeletal muscle (Table S6) and highlighted
211 the top 10 proteins with the highest acetyl-intensity (Fig. 4C). Histone H4 (HIST1H4A) had the
212 highest acetylation intensity, making up approximately 10% of the total acetylome intensity,
213 supporting the regulatory role of histone acetylation in modulating transcription[48,49]. The majority of
214 the remaining top acetylated proteins were metabolic enzymes, including the TCA cycle proteins
215 malate dehydrogenase (MDH2) and fumarate hydratase (FH), as well as subunits of complex V
216 (ATP5H and ATP5O) within the electron transport chain. Superoxide dismutase (SOD2), a canonical
217 acetylated enzyme involved in mitochondrial reactive oxygen species handling[50,51], also displayed
218 high acetylation intensity. We further compared the protein abundance rank for these high-intensity
219 acetylated proteins within the proteome (Fig. 4D). These proteins did not appear to be the highest
220 intensity acetylated proteins simply due to their relative protein abundance. While they all fell within
221 the top 318 proteins in the proteome, they did not make up the most abundant proteins, except for
222 creatine kinase M-type (CKM), which is extremely abundant in skeletal muscle (Fig. 4D). To identify
223 systematic trends in protein acetylation, we performed a one-dimensional enrichment analysis[52] on
224 the summed protein acetylation intensities, which ranked the proteins by acetylation intensity and
225 identifies Gene Ontology (GO) annotations that are systematically over-represented with higher

226 intensities (positive enrichment factor) and lower intensities (negative enrichment factor). This
227 identified mitochondrial terms (e.g. GOCC: mitochondrial part and mitochondrial matrix) as enriched
228 for high acetylation intensity (Fig. 4E and Table S7). In particular, proteins of carboxylic acid
229 metabolic processes (e.g. TCA cycle) and monovalent inorganic cation transport (e.g. electron
230 transport chain complex V proteins) display systematically high acetylation intensity (Fig.4E and
231 Table S7). Furthermore, the Uniprot keyword term "muscle protein" was also enriched for high
232 acetylation intensity, a term that mainly encompasses the contractile machinery of skeletal muscle
233 (e.g. myosins).
234
235 In order to examine acetylation stoichiometry within skeletal muscle, we estimated the relative
236 stoichiometries of acetyl-sites using abundance-corrected intensities (ACI) (Table S8). ACIs were
237 calculated by dividing acetyl-peptide intensities by the intensities of their corresponding protein, with
238 ACI values correlating with stoichiometry[15]. After ranking acetyl-site ACI for the pre-HIIT samples,
239 we highlighted the top 10 acetyl-sites with the highest ACI (Fig. 4F). Trifunctional enzyme subunit
240 alpha (HADHA), FH, HIST1H4A and 3- ketoacyl-CoA thiolase (ACAA2), which were identified as
241 among the highest intensity acetylated proteins (Fig. 4C), all contain high stoichiometry acetyl-sites
242 (Fig. 4F). However, nicotinamide nucleotide transhydrogenase (NNT) K70 had the highest ACI
243 within skeletal muscle (Fig. 4F). NNT is an inner mitochondrial membrane protein, which uses the
244 proton motive force to maintain high levels of NADPH (Hoek and Rydström, 1988) and in doing so
245 can regulate metabolism[53,54]. NNT is also highly acetylated in cardiac muscle[55], although the effect
246 of acetylation on NNT activity remains to be determined. Nonetheless, NNT can regulate acetylation
247 via NADPH-mediated regulation of histone deacetylase 1 (HDAC1) activity[54], thus acetylation of
248 NNT may represent a feedback mechanism controlling cellular acetylation and metabolism.
249

250 To identify systematic trends in acetyl-site stoichiometry, we performed a one-dimensional
251 enrichment analysis[52] on acetyl-site ACI using the leading protein ID for relative enrichment[56]. We
252 identified the mitochondria (e.g. GOCC: mitochondrial part and mitochondrial inner membrane) and
253 carboxylic acid catabolic processes to be enriched within higher stoichiometry acetylated proteins
254 (Figs. 4G, 4H & Table S9). This extends previous analyses by not only showing that mitochondrial
255 proteins make up the majority of acetylated proteins in skeletal muscle[18], but also by identifying
256 mitochondrial proteins as having relatively high stoichiometry acetyl-sites – an observation that is
257 consistent with analyses in HeLa cells, rodent liver and yeast[15,21,57]. Enriched for proteins with low
258 stoichiometry acetyl-sites were proteins involved in contraction (e.g. GOCC: contractile fiber part;
259 Figs. 4G, 4H & Table S9), including the Uniprot keyword term "muscle protein" (Fig. 4G), which,
260 conversely, was enriched for high protein acetylation intensity (Fig. 4E). Myosin displayed the
261 greatest enrichment for low acetylation stoichiometry (Fig. 4G). Thus, despite contractile proteins
262 displaying high protein acetylation intensity and making up a substantial number of known acetylated
263 proteins within skeletal muscle[18], they contain acetylation sites of relatively low stoichiometry. The
264 high acetylation intensity of these proteins is therefore likely due to high protein abundance and a
265 large number of acetylation sites per protein. Proteins annotated to the cytosol and plasma membrane
266 also displayed low acetyl-site ACI (Fig. 4G). This highlights differences in the inter-organelle
267 acetylation levels of skeletal muscle and can likely be explained by subcellular compartmentalization
268 of acetyl-CoA[58].
269

270 **HIIT induces acetylation of mitochondrial and TCA cycle proteins**

271 HIIT increased the mean number of acetyl-sites quantified per sample by over 100 sites (Pre: 915 ±
272 44, Post: 1037 ± 51; $p = 0.015$; Fig. S4B). Using a stringent statistical approach of permutation-based
273 FDR corrected paired t-tests, we identified 20 upregulated acetyl-sites and 1 downregulated site (FDR

274 < 0.05; Fig. 4A). In addition, by applying a validated, albeit less stringent, significance score (Π-
275 value), which combines the statistical significance (p-value) with the fold change[59], we extended this
276 to identify 257 upregulated and 26 downregulated acetyl-sites following HIIT (Π < 0.05; Fig. 5A and
277 Table S5). In general, there was a trend for increased acetylation following HIIT (Fig. 4A), which
278 could not be explained by changes in protein content as the fold changes in acetylation generally
279 exceeded those of protein abundance (Fig. 5B). Therefore, we did not normalize the acetylome data
280 to protein abundance. Within the increased sites, acetyl-sites on metabolic enzymes isocitrate
281 dehydrogenase (IDH2), succinate CoA ligase subunit alpha (SUCLG1) and ATP synthase coupling
282 factor 6 (ATP5J) were apparent (Fig. 5A), while hyperacetylation of SOD2 occurred at K68, 75, 122
283 and 130 in response to HIIT (Fig. 5A). Included within the downregulated sites were acetyl-sites on
284 annexin A6 (ANXA6), laminin (LMNA) and p38 mitogen-activated protein kinase γ (MAPK12) (Fig.
285 5A). Interestingly, Histone H1.5 (HIST1H1B) K49 showed increased acetylation, despite
286 significantly reduced protein abundance (Fig. 5B).
287
288 A Fisher's exact test of HIIT-regulated acetyl-sites (Π < 0.05), using leading protein ID for relative
289 enrichment, indicated the predominant regulation of the TCA cycle pathway, mitochondrial proteins
290 (e.g. GOCC: mitochondrial part and mitochondrial inner membrane) and, in particular, electron
291 transport chain complex V proteins (GOCC: mitochondrial proton-transporting ATP synthase
292 complex) (Fig. 5C, Table S10). These GO terms were strikingly similar to the terms enriched for high
293 acetylation intensity and stoichiometry in the pre-HIIT samples (Figs. 4E and G), indicating that
294 proteins that are highly acetylated in the basal state are most susceptible to increased acetylation
295 following HIIT. To further explore the regulation of HIIT-induced acetylation in skeletal muscle, we
296 looked for consensus sequences around the acetylated lysine residues using iceLogo[60]. We identified
297 a sequence with a predominance of proximal cysteine residues as well as an aspartic acid residue in

298 the +1 position (Fig. 5D). The aspartic acid at +1 is a feature of mitochondrial acetylated proteins[18]
299 and its enrichment is likely due to the over-representation of mitochondrial proteins in the upregulated
300 acetyl-sites (Fig. 5C). Proximal cysteine residues are associated with promoting non-enzymatic lysine
301 acetylation[15,61] via initial cysteine acetylation followed by transfer of the acetyl group to lysine[61].
302 Indeed, non-enzymatic acetylation increases alongside elevated fatty acid oxidation[20], as is apparent
303 in skeletal muscle mitochondria after HIIT (Figs. 1E). This likely occurs through changes in acetyl-
304 CoA concentration and/or increased acetyl-CoA flux[20]. Although acetyl-CoA content within resting
305 skeletal muscle does not change in response to exercise training[62], acetyl-CoA levels and TCA cycle
306 flux increase during exercise[62-65], which may result in an accumulation of lysine acetylation during
307 repeated bouts of exercise. Conversely, acute exercise decreases skeletal muscle acetylation in
308 exercising rats[12], but whether this is the case for humans remains to be determined. Nonetheless, we
309 identify a robust increase in skeletal muscle acetylation, predominantly of mitochondrial proteins,
310 following five weeks of HIIT in humans.
311
312 Because HIIT altered the skeletal muscle acetylome, we examined proteins regulating deacetylases
313 following HIIT. Sirtuin 1 (SIRT1), a nuclear and cytosolic deacetylase, was not quantified by mass
314 spectrometry, and a small but non-significant trend for increased expression of the mitochondrial-
315 localized sirtuin 3 (SIRT3) was apparent (Table S2). To further investigate this, we immunoblotted
316 for SIRT1 and SIRT3. Expression of SIRT1 did not change, while SIRT3 increased in abundance
317 following HIIT (Fig. 5E). Thus, mitochondrial acetylation increased concomitantly with an increase
318 in the mitochondrial deacetylase (Figs. 5B and 5E). Indeed, SIRT3 appears to play a major role in
319 suppressing non-enzymatic mitochondrial acetylation[21]. Therefore, the elevated SIRT3 abundance
320 following exercise training might be interpreted as a mechanism to suppress excess acetylation, either
321 to preserve the activity of mitochondrial enzymes[66-68] or to scavenge acetyl groups for reintegration

322 into acetyl-CoA and energy production. Altogether, the data contained within Fig. 5 indicate a
323 predominantly non-enzymatic acetylation of mitochondrial proteins during HIIT.
324
325 Given the enrichment of mitochondrial terms and particularly of complex V proteins in the HIIT-
326 regulated acetylated proteins, we filtered for proteins annotated to the different complexes of the
327 electron transport chain using the HUGO database[69] and highlighted the regulation of each acetyl-
328 site on these proteins alongside the changes in protein abundance (Fig. 6A). While proteins of
329 complexes I, II, III and IV showed a mixed acetylation response to exercise training, almost every
330 quantified complex V protein had at least one acetyl-site that increased following HIIT (Fig. 6A). In
331 fact, ATPase inhibitor (ATPIF1), one of the two complex V proteins that do not show elevated
332 acetylation, is a negative regulator of complex V and is unlikely to be constitutively bound to the
333 ATP synthase complex[70]. Why complex V displays elevated acetylation levels both in the basal (Fig.
334 4E) and exercise trained states is unclear (Figs. 5C and 6A). However, as a large proportion of ATP
335 synthase extends into the mitochondrial matrix, many subunits are likely to be more exposed to
336 acetyl-CoA than other membrane-embedded electron transport chain complexes. In support, we
337 detected acetylation on all of the subunits of complex V that reside or extend into the mitochondrial
338 matrix (ATP5A1, ATP5B, ATP5C1, ATP5D, ATP5E, ATP5F1, ATP5H, ATP5J and ATP5O), while
339 we only detect acetylation on two of the membrane-embedded subunits (ATP5L and MT-ATP8),
340 despite detecting a further four membrane-embedded subunits in the proteome (ATP5I, ATP5J2, MT-
341 ATP6 and USMG5). Indeed, the majority of acetylated proteins quantified on each electron transport
342 chain complex (CI-CV) are exposed to either the mitochondrial matrix or the intermembrane space.
343 Similarly, TCA cycle enzymes, which are localized to the mitochondrial matrix, displayed high
344 acetylation intensity and stoichiometry in the basal state and HIIT augmented levels of acetylation at
345 every stage of the cycle (Fig. 6B), again likely due to their proximity to acetyl-CoA. Conversely,

346 cytosolic proteins regulating skeletal muscle contraction showed fewer upregulated acetyl-sites with
347 a number of downregulated sites following HIIT (Fig. 6C). Thus, proteins in close proximity to
348 acetyl-CoA appear to be more susceptible to acetylation.
349
350 Despite widespread HIIT-induced acetylation of mitochondrial proteins, these data should be
351 considered in the context of acetylation stoichiometry, which is generally low[21]. Median acetylation
352 stoichiometry in rodent liver has been calculated at only 0.05%, which increases slightly to 0.11%
353 for mitochondrial proteins[21]. Although acetylation is tissue-dependent[18], skeletal muscle levels are
354 unlikely to be vastly different. The median log_2-fold change for mitochondrial acetyl-sites following
355 HIIT was 0.9 (the corresponding value in the proteome was 0.3), indicating that median post-HIIT
356 stoichiometry would have remained at less than 1%. Even for the acetyl-sites with the greatest fold
357 change in our dataset, which display log_2-fold changes in the order of 4-5 (Figs. 5A and 5B), post-
358 HIIT stoichiometry will likely be in the single figure percentages. Thus, the levels of HIIT-induced
359 changes in acetylation may not be large enough to influence gross activity on most metabolic
360 enzymes. Indeed, hyperacetylation has limited impact on mitochondrial bioenergetics within murine
361 skeletal muscle, although severe hyperacetylation increases long-chain fatty acid-supported
362 respiration[22]. These data are consistent with the concomitant increase in acetylation (Fig. 5A) and
363 mitochondrial respiratory capacity (Fig. 1F) following HIIT.
364
365 **HIIT increases histone acetylation**
366 Aside from metabolic enzymes and contractile proteins, histones are regulated by acetylation[48,49] and
367 may represent a more specifically regulated pool of proteins, owing to the nuclear localization of
368 acetyltransferases[71]. Increases in certain acetylated histone residues are well characterized to augment
369 transcription, with exercise known to acutely regulate H3 acetylation (e.g. H3 K4, H3 K9/14 & H3

370 K36)[72-75]. Here we identified 18 distinct acetylated peptides from histones, with acetylated peptides
371 from H1.5 (HIST1H1B K48), H2B type 2F (HIST2H2BF K16/20) and H3.3 (H3F3B K23) being
372 elevated following HIIT (Figs. 7A-D). H1.5 K48 was exclusively quantified in post-HIIT samples,
373 however, it was only quantified in 4 out of 7 of the post-HIIT samples, which is our minimum cut off
374 for valid values. The regulatory roles of these HIIT-regulated histone acetyl-sites are unknown.
375 However, acetylation of the N-terminal of H2B, including K16 & K20, has been linked to
376 transcriptional activation[76,77], including the expression of NAD-metabolic genes in yeast[77]. The role
377 of H3 K23 is also obscure, however, its acetylation contributes to the development of cancer through
378 the recruitment of the transcription factor transcription intermediary factor 1-alpha (TRIM24) and the
379 nuclear receptor estrogen receptor alpha (ERS1)[78,79], augmenting expression of phosphatidylinositol
380 4,5-biphosphate 3-kinase catalytic subunit alpha (PIK3CA), a subunit of phosphoionositide-3-kinase
381 (PI3K), and phosphorylation of protein kinase B (AKT1)[78]. Indeed, TRIM24 promotes the expression
382 of glycolytic and TCA cycle genes in transforming human mammary epithelial cells[80], while ERS1
383 regulates mitochondrial biogenesis in skeletal muscle[81]. Whether H3 K23 regulates TRIM24, ERS1,
384 PI3K, and AKT1 activity and influences metabolism in skeletal muscle remain unclear. Further
385 studies are warranted to understand the transcriptional and metabolic implications of exercise
386 training-induced acetylation on these histone sites.
387

388 **Conclusion**

389 Here, we leveraged advances in DIA mass spectrometry to produce the largest single-shot human
390 skeletal muscle proteome to date and applied this approach to ascertain exercise training adaptations.
391 Furthermore, we provide the first investigation of the human acetylome in response to exercise
392 training. In the proteome, we highlight known and novel exercise-responsive proteins, including a
393 potential mechanism to explain altered skeletal muscle calcium sensitivity following HIIT. In the

394 acetylome, we describe the predominant acetylation of mitochondrial proteins after HIIT, particularly
395 of TCA cycle proteins and subunits of electron transport chain complex V, as well as highlighting the
396 regulation of novel exercise-responsive histone acetyl-sites. Altogether, we provide a substantial
397 hypothesis-generating resource, identifying novel exercise-regulated proteins and acetyl-sites with
398 the aim of stimulating further mechanistic research investigating how exercise improves metabolic
399 health.
400

401 **Methods**

402 *Participants*

403 Eight men gave their informed consent after receiving written and oral information about the study
404 and potential risks associated with the experimental procedures. Inclusion criteria were healthy males,
405 18-40 years old, maximal oxygen consumption ($\dot{V}O_{2max}$) between 45-55 $mL \cdot min^{-1} \cdot kg^{-1}$ or 3000-
406 4000 $mL \cdot min^{-1}$ and BMI between 19-26 $kg \cdot m^{-2}$. Exclusion criteria were abnormal
407 electrocardiogram, chronic disease, ongoing medical treatment, and smoking. Subject characteristics
408 are presented in Table 1. The study was approved by the National Committee on Health Research
409 Ethics (H-17004045) and registered at clinicaltrials.gov (NCT03270475). The study complied with
410 the Declaration of Helsinki (2013).
411

412 *Experimental trials*

413 The study consisted of two experimental days separated by five weeks of high-intensity interval
414 training (HIIT). At each experimental day, body composition was measured by dual-energy X-ray
415 absorptiometry (DXA) scans (Lunar iDXA, GE Healthcare, GE Medical systems, Belgium). Then,
416 subjects rested in a supine position for 15 min and two 4 mm incisions separated by 2 cm were made

417 in the above the *vastus lateralis* muscle under local anaesthesia (Xylocaine 20 mg · mL^{-1} without
418 epinephrine, AstraZeneca, London, UK) and a muscle biopsy was taken from each incision using a
419 Bergström needle with suction. Afterwards, $\dot{V}O_{2max}$ was determined by indirect calorimetry using a
420 breath-by-breath gas analyser (Oxycon Pro, CareFusion, San Diego, USA) during an incremental test
421 on a bike ergometer (Monark LC4, Monark Exercise, Vansbro, Sweden). The incremental test
422 consisted of 5 min rest followed by 4 min stages at 50, 100, 150 W, after which the resistance was
423 increased in increments of 30 W·min^{-1} until exhaustion. Time to exhaustion was used to calculate
424 incremental peak power output (iPPO) accounting for time spent at the last increment. Subjects
425 completed the experimental protocol the same time of day before and after the intervention and were
426 instructed to eat a small meal with 500 mL water two hours before arriving at the laboratory. In
427 addition, subjects abstained from alcohol, caffeine, and physical activity for 48 h before each
428 experimental day and were instructed to maintain their activity level and diet during the study. The
429 experimental days were performed three days before and after the first and last training, respectively.
430

431 *Body composition*

432 At each experimental day, two scans were performed to reduce scan-to-scan variation[82]. Before the
433 first scanning, subjects rested in a supine position for 10 min to allow fluid distribution reducing intra-
434 scan variation[83,84]. Whole-body and leg composition were calculated using software (enCORE Forma
435 v. 15, GE Healthcare Lunar, Buckinghamshire, UK).
436

437 *Substrate utilization*

438 Gas exchange measurements during rest and submaximal exercise were used to calculate fat and
439 glucose oxidative as previously described[85] and corrected for protein oxidation[86]. Fat oxidation and
440 carbohydrate oxidation were calculated as:

441 $$Fat\ Oxidation\left(\frac{mg}{min}\right) = \left(1.695 \cdot \dot{V}O_2 - 1.701 \cdot \dot{V}CO_2\right) - \frac{1.92 \cdot 0.14 \cdot BM}{1440}$$

442 $$Carbohydrate\ Oxidation\left(\frac{mg}{min}\right) = \left(4.344 \cdot \dot{V}CO_2 - 3.061 \cdot \dot{V}O_2\right) - \frac{2.87 \cdot 0.14 \cdot BM}{1440}$$

443 where $\dot{V}O_2$ and $\dot{V}CO_2$ are in L·min^{-1} and *BM (Body mass)* is in kg.

444

445 *Muscle biopsies*

446 Immediately after collection, muscle biopsies were rinsed in ice-cold saline. A small piece (~15 mg)
447 of the muscle was transferred into ice-cold preservation solution (BIOPS) for analysis of
448 mitochondrial respiratory capacity. The remaining muscle tissue was snap-frozen in liquid nitrogen
449 and stored at –80°C. The frozen muscle samples were freeze-dried for 48 h and dissected free from
450 connective tissues, fat and blood under a microscope in a humidity-controlled room (~25% humidity)
451 before storage at –80°C for later analyses.

452

453 *High intensity interval training*

454 Subjects underwent a five-week high-intensity interval training intervention consisting of three
455 weekly training sessions with 4-5 × 4 min intervals interspersed by two min active recovery on indoor
456 spinning bikes. The training volume increased from four intervals during the first two weeks to five
457 intervals during the last three weeks. During each interval, subjects were instructed to reach >90% of
458 maximal heart rate (HR_{max}). All training sessions were supervised and subjects received verbal
459 encouragement during all intervals. The mean HR_{max} during intervals was 96 ± 1% of HR_{max}.

460

461 *Mitochondrial profiling*

462 Mitochondrial respiratory capacity was determined in duplicate by high-resolution respirometry
463 (Oxygraph-2k, Oroboros Instruments, Innsbruck, Austria) at 37°C using 1-3 mg wet weight muscle

464 fibers per chamber in MiR06. Oxygen concentrations were kept between 200 and 450 µM throughout
465 the experiment. The muscle sample in BIOPS was prepared for high-resolution respirometry as
466 previously described[87]. In short, muscle fibers were dissected free from connective tissue and fat
467 followed by permeabilization in BIOPS with saponin and washed in mitochondrial respiration buffer
468 (MiR06). A substrate-uncoupler-inhibitor titration protocol was used to assess different respiratory
469 states as previously described[27]. Leak respiration (L_N) in the absence of adenylates was induced by
470 the addition of malate (2 mM) and octanoylcarnitine (0.2 mM). Fatty acid oxidation (FAO) was
471 determined after titration of ADP (2.5 mM). Submaximal CI and CI+II-linked respiration (CI_D & P_D)
472 was measured in the presence of glutamate (10 mM) and succinate (10 mM), respectively. Oxidative
473 phosphorylation capacity (P) was assessed after another titration of ADP (2.5 mM). The
474 mitochondrial outer membrane integrity was then tested with the addition of cytochrome C (10 µM).
475 The average change in oxygen flux was 3.8% (range: 0.2-9.4%). Respiratory electron transfer-
476 pathway capacity (E) was measured during step-wise (0.5 µM) titration of carbonyl cyanide p-
477 trifluoro-methoxyphenyl hydrazine (FCCP). Succinate-supported electron transfer-pathway capacity
478 (E_{CII}) was assessed by the addition of rotenone (0.5 µM). Residual oxygen consumption was
479 determined after the addition of malonic acid (5 mM), myxothaizol (0.5 µM) and antimycin A (2.5
480 µM) and subtracted from each respiratory state.
481
482 Maximal enzyme activity of citrate synthase was determined from muscle homogenate using
483 fluorometry (Fluoroscan Ascent, Thermo Fisher Scientific, Waltham, USA) at 25°C as previously
484 described[88].
485
486 *Proteomic sample preparation*

487 Human skeletal muscles were lysed in a buffer consisting of 1% Sodium Deoxycholate (SDC), 10
488 mM Tris (2-carboxyethyl) phosphine (TCEP), 40 mM Chloroacetamide (CAA) and 100 mM of Tris
489 (pH 8.5). The muscles were homogenized with an Ultra Turrax homogenizer (IKA). Lysates were
490 boiled at 95°C for 10 min and sonicated using a tip sonicator. Lysates were then centrifuged at 16000g
491 for 10 min. Proteins were digested using the endoproteinases LysC and trypsin (1:100 w/w) at 37°C
492 overnight with shaking. Digested peptides were acidified using 1% Trifluoroacetic acid (TFA) and
493 precipitated SDC was removed by centrifugation. Peptides were purified using Sep-pak C18
494 cartridges (Waters) and were eluted in 50% acetonitrile. 20 µg of peptides were saved for total
495 proteome analysis while 3 mg peptides were saved for enrichment of acetylated peptides.
496
497 *Acetylated peptide enrichment*
498 The acetyl peptide enrichment was performed on 3 mg of digested peptides using PTMscan Acetyl-
499 Lysine Motif kit (Cell Signaling #13416). The peptides were mixed with 100 µL of 10x IP buffer
500 (500 mM MOPS, pH 7.2, 100 mM Na-phosphate, 500 mM NaCl, 5% NP-40). The acetonitrile was
501 removed and the volume was reduced to ~1mL by vacuum centrifugation. The final volume was
502 adjusted with water to a concentration of 3 $mg \cdot mL^{-1}$. The peptides were clarified by centrifugation at
503 20000g for 5 min. 20 µL of anti-acetylated lysine antibody was washed 3 times in 1 mL IP buffer and
504 then mixed with the peptides. Peptides were enriched overnight at 4°C, washed 3 times in 1 mL ice-
505 cold (4°C) IP buffer, 4 times in 1 mL ice-cold IP buffer without NP-40, and once in 1 mL water. All
506 wash buffer was removed via aspiration. Acetylated peptides were eluted with 100 µL 0.15% TFA.
507 The elution procedure was repeated three times. The eluted peptides were de-salted on C18 stage-
508 tips[89], vacuum concentrated and resuspended in buffer A* (5% acetonitrile, 0.1% trifluoroacetic acid).
509
510 *High pH reversed-phase fractionation*

511 To generate a deep proteome library for data-independent acquisition (DIA), 50 µg of peptide was
512 pooled from pre- and post-HIIT samples, separately, and fractionated using high pH reversed-phase
513 chromatography[90]. 24 fractions (per pool) were automatically concatenated using a rotor valve shift
514 of 90 s. Approximately 0.3 µg of each fraction were subjected to LC-MS/MS measurements via data-
515 dependent acquisition (DDA). To obtain comprehensive coverage of the acetylome, acetylated
516 peptides from each sample were fractionated into 8 fractions using a rotor valve shift of 90 s. For the
517 first subject (both pre and post samples) all 8 fractions were analysed separately. After observing
518 lower than expected peptide intensities for the first subject, the neighboring two factions were pooled
519 together for each of the remaining samples (total four fractions/subject/timepoint) before LC-MS
520 analysis.
521
522 *Mass spectrometry*
523 Peptides were measured using LC-MS instrumentation consisting of an Easy nanoflow HPLC system
524 (Thermo Fisher Scientific, Bremen, Germany) coupled via a nanoelectrospray ion source (Thermo
525 Fischer Scientific, Bremen, Germany) to a Q Exactive HF-X mass spectrometer. Purified peptides
526 were separated on a 50 cm C18 column (inner diameter 75 µm, 1.8 µm beads, Dr. Maisch GmbH,
527 Germany). Peptides were loaded onto the column with buffer A (0.5% formic acid) and eluted with
528 a 100 min linear gradient increasing from 2-40% buffer B (80% acetonitrile, 0.5% formic acid). After
529 the gradient, the column was washed with 90% buffer B and re-equilibrated with buffer A.
530
531 For the deep proteome library generation, mass spectra were acquired from each fraction via DDA
532 with automatic switching between MS and MS/MS using a top 15 method. MS spectra were acquired
533 in the Orbitrap analyzer with a mass range of 300-1750 m/z and 60,000 resolutions at m/z 200 with
534 a target of 3 x 10^6 ions and a maximum injection time of 25 ms. HCD peptide fragments acquired at

535 27 normalized collision energy were analyzed at 15000 resolution in the Orbitrap analyzer with a
536 target of 1 x 105 ions and a maximum injection time of 28 ms. The mass spectra for the acetylome
537 experiments were also acquired from each fraction via DDA with a similar MS method used for deep
538 proteome library generation, except the maximum injection time for the fragment ion spectra was set
539 to 250 ms. A DIA MS method was used for the total proteome measurements in which one full scan
540 (300 to 1650 *m/z*, resolution = 60,000 at 200 *m/z*) at a target of 3 x 10^6 ions was first performed,
541 followed by 32 windows with a resolution of 30000 where precursor ions were fragmented with
542 higher-energy collisional dissociation (stepped collision energy 25%, 27.5%, 30%) and analyzed with
543 an AGC target of 3 x 10^6 ions and maximum injection time at 54 ms in profile mode using positive
544 polarity.
545
546 *Data processing*
547 Raw MS files from the experiments measured in DDA mode (muscle proteome library & acetylome),
548 were processed using MaxQuant[91]. MS/MS spectra were searched by the Andromeda search engine
549 (integrated into MaxQuant) against the decoy UniProt-human database (downloaded in December
550 2017) with forward and reverse sequences. In the main Andromeda search precursor, mass and
551 fragment mass were matched with an initial mass tolerance of 6 ppm and 20 ppm, respectively. The
552 search included variable modifications of methionine oxidation and N-terminal acetylation and fixed
553 modification of carbamidomethyl cysteine. For the raw files from the acetylome experiments,
554 acetylated lysine was also added as a variable modification. Acetylated peptides were filtered for a
555 minimum Andromeda score of 40, as per the default settings for modified peptides. The false
556 discovery rate (FDR) was estimated for peptides and proteins individually using a target-decoy
557 approach allowing a maximum of 1% false identifications from a revered sequence database. Raw
558 files acquired in the DIA mode (total proteome) were processed using Biognosys Spectronaut

559 software version 13[92]. A single peptide library was generated in Spectronaut using the combined
560 MaxQuant search results for the DDA runs from both of the fractionated muscle samples. The
561 experimental DIA runs were then analyzed in Spectronaut using default settings.
562
563 *Bioinformatics*
564 Bioinformatic analyses were performed in the Perseus software[56]. Categorical annotations were
565 supplied in the form of Gene Ontology (GO) biological process (BP), molecular function (MF), and
566 cellular component (CC), as well as UniProt Keywords, KEGG and REACTOME pathways. All
567 annotations were extracted from the UniProt database. Quantified proteins were filtered to have at
568 least 4 valid values in at least one time point. Missing data were imputed by drawing random numbers
569 from a Gaussian distribution with a standard deviation of 30% and a downshift of 1.8 standard
570 deviations from the mean. The imputed values have been tuned in order to simulate the distribution
571 of lowly abundant proteins. To identify differentially regulated proteins and acetyl-sites, two-tailed
572 paired *t*-tests were performed with a permutation-based false discovery correction applied (FDR =
573 0.05). In the acetylome, an additional analysis was performed to expand the identification of
574 differentially expressed proteins, whereby an *a posteriori* information fusion scheme combining the
575 biological relevance (fold change) and the statistical significance (p-value), was implemented, as
576 previously described[59]. A Π-value significance score cut-off of 0.05 was selected. Alterations to
577 organelles were assessed using summed total protein abundances[93] and two-tailed paired t-tests ($p <$
578 0.05). Comparisons between individual proteins measured via immunoblotting were performed using
579 two-tailed paired t-tests ($p < 0.05$). Hierarchical clustering analysis was performed on z-scored
580 differentially regulated proteins using Euclidean distance. Enrichment analyses were performed on
581 differentially regulated proteins and acetyl-sites using Fisher's exact tests and the application of a
582 Benjamini-Hochberg false discovery correction (FDR = 0.02). Motif enrichment was performed on

583 upregulated acetyl-sites using iceLogo ($p < 0.01$)[60]. One-dimensional enrichment analyses were
584 performed as previously described[52]. To analyze the relative stoichiometries of acetylated proteins in
585 Fig. 4 abundance corrected intensities (ACIs) were calculated for each acetyl-peptide by dividing the
586 acetyl-peptide intensity by the intensity of the corresponding protein in the proteome. Enrichment
587 analyses were performed against a background of all quantified proteins or acetyl-sites, except for
588 hierarchical clustering analyses where clusters were compared within the z-scored differentially
589 regulated matrix. To visualize complexes and functional protein-interactions in Fig. 6, protein
590 interaction networks were mapped using the STRING database, using an overall confidence cutoff of
591 0.7 without limiting the number of interactions[94], and further processed with Cytoscape
592 (www.cytoscape.org).
593
594 *Immunoblotting*
595 A fresh batch of ice-cold homogenization buffer (10% glycerol, 20 mM Na-pyrophosphate, 150 mM
596 NaCl, 50 mM HEPES (pH 7.5), 1% NP-40, 20 mM β-glycerophosphate, 2 mM Na_3VO_4, 10 mM NaF,
597 2 mM PMSF, 1 mM EDTA (pH 8), 1 mM EGTA (pH 8), 10 $\mu g \cdot mL^{-1}$ Aprotinin, 10 $\mu g \cdot mL^{-1}$
598 Leupeptin and 3 mM Benzamidine) was prepared and 80 µL added to 1 mg of freeze dried and
599 dissected muscle tissue. The tissue was homogenized for 1 min at 28.5 Hz in a TissueLyser (Qiagen
600 TissueLyser II, Retsch GmbH, Germany) before samples were rotated end over end for 1 hour at 4°C
601 and centrifuged at 18320g for 20 min at 4°C. The pellet was discarded and the supernatant was taken
602 and used for immunoblotting analyses. Total protein concentration in the samples was determined
603 with a standard BSA kit (Millipore). 15 µL of the sample was diluted with 60 µL ultrapure water in
604 order to keep the concentration within the linear range of the calibration curve (0.2 to 2 $\mu g \cdot \mu L^{-1}$). The
605 protein concentration of each sample was adjusted by the addition of 6 × Laemmli buffer (7 mL 0.5M
606 Tris-base, 3 mL glycerol, 0.93 g DTT, 1 g SDS and 1.2 mg bromophenol blue) and ultrapure water

607 to reach equal concentrations (1.5 µg total protein·μL^{-1}). Human skeletal muscle standard samples
608 (Ctrl) were obtained as a pool of all samples included in the experiment.
609
610 Equal amounts of total protein were loaded on 10% TGX Stain-Free or 16.5% Criterion Tris-
611 Tricine/Peptide gels (Bio-Rad) alongside two protein markers (Precision plus all blue and dual color
612 standards, Bio-Rad), three human skeletal muscle control samples and a four-point standard curve
613 (skeletal muscle samples of increasing volume). After standard SDS-page gel electrophoresis proteins
614 were semi-dry transferred to a PVDF membrane. Membranes were blocked with either 2% skimmed
615 milk or 3% BSA in Tris-buffered saline with 0.1% Tween-20 (TBST) before overnight incubation
616 with primary antibody. Afterwards, the membranes were washed in TBST, incubated for 1 hour in
617 HRP conjugated secondary antibody at room temperature and washed 3 × 15 min in TBST before the
618 bands were visualized with an enhanced chemiluminescent reaction (Immobilon Forte Western HRP
619 substrate, Millipore) and signals recorded with a digital camera (ChemiDoc MP Imaging System,
620 Bio-Rad). Densitometry quantification of the immunoblotting band intensities was done using Image
621 Lab version 4 (Bio-Rad) and determined as the total band intensity adjusted for the background
622 intensity. The standard curve on each gel was used to confirm that the loaded amount of protein in
623 samples was capable of determining differences between samples by the signal intensity being on the
624 linear part of the standard curve. The variation of the triplicate human standard sample signal loaded
625 was used to evaluate equal transfer of proteins across each gel. Coomassie staining was conducted to
626 confirm equal loading and transfer of total protein from the different samples.
627
628 Listed are the primary antibodies used and their size of migration. MFN2: #11925, Cell Signaling
629 Technologies, 80 kDa; MYLK2: PA5-29324, Invitrogen, 65 kDa; NAMPT: A300-779A, Bethyl
630 Laboratories, 56 kDa; OXPHOS antibody cocktail: ab110411, Abcam, 15-55 kDa; SIRT-1: 07-131,

631 Millipore, 80 kDa; SIRT-3: #5490, Cell Signaling Technologies, 28 kDa; SIRT-5: #8782, Cell
632 Signaling Technologies, 30 kDa; HRP conjugated goat anti-rabbit (4010-05, SouthernBiotech) and a
633 goat anti-mouse (P0447, DAKO Denmark) were used as secondary antibodies.
634
635 *Statistical analyses*
636 For non-omics analyses, two-tailed paired t-tests were applied to assess the effect of HIIT, except for
637 substrate oxidation analyses whereby a mixed linear model was performed ($p < 0.05$).
638

Acknowledgements

This work was supported by an unconditional donation from the Novo Nordisk Foundation (NNF) to NNF Center for Basic Metabolic Research (http://www.cbmr.ku.dk) (Grant number NNF18CC0034900), NNF Center for Protein Research (https://www.cpr.ku.dk/) (Grant number NNF14CC001), and Team Denmark. We would like to acknowledge Matthias Mann, Jens Jung Nielsen, Rebeca Soria Romero and the mass spectrometry platform from at the NNF Center for Protein Research for technical assistance and access to mass spectrometers.

Author contributions

Conceptualization: M.H., A.S.D., A.K.L. and J.B. **Data curation**: A.S.D., M.H., A.K.L. and B.S. **Formal analysis**: B.S., A.K.L., M.H., M.T., J.K.L. and A.S.D. **Funding acquisition**: A.S.D., M.H. and J.B. **Investigation**: B.S., A.K.L., M.H., M.T., A.G., J.K.L. and A.S.D. **Methodology**: M.H., A.S.D., A.K.L., B.S., J.K.L., A.G. and J.B. **Project administration**: M.H. and A.S.D. **Resources**: A.S.D., M.H. and J.B. **Supervision**: A.S.D. and M.H. **Validation**: M.T., B.S., A.K.L., M.H. and A.S.D. **Visualization**: B.S. **Writing – Original draft**: B.S., M.H., A.K.L. and A.S.D. **Writing – review and editing**: M.H., A.K.L., B.S., A.G., J.K.L. M.T., B.W., J.B. and A.S.D.

Competing interests

The authors declare no competing interests.

Materials & Correspondence

Requests for reagents and resources should be directed to Atul S. Deshmukh (atul.deshmukh@sund.ku.dk).

664 **Supplementary Tables**

665 ***Table S1.*** *Identified proteins.*

666

667 ***Table S2.*** *Quantified proteins and their regulation by HIIT.*

668

669 ***Table S3.*** *Fisher's exact test of HIIT-regulated proteins (FDR < 0.05).*

670

671 ***Table S4.*** *Identified acetyl-sites.*

672

673 ***Table S5.*** *Quantified acetyl-sites and their regulation by HIIT.*

674

675 ***Table S6.*** *Summed acetylation intensity per protein.*

676

677 ***Table S7.*** *One-dimensional enrichment analysis of summed acetylation intensity.*

678

679 ***Table S8.*** ***A****bundance corrected intensities (ACIs) of acetyl-sites pre-HIIT.*

680

681 ***Table S9.*** *One-dimensional enrichment analysis of pre-HIIT acetyl-site ACI (Leading protein IID*

682 *was used for relative enrichment).*

683

684 ***Table S10.*** *Fisher's exact test of HIIT-regulated (TI < 0.05) acetyl-sites (Leading protein IID was*

685 *used for relative enrichment).*

686

687 *https://drive.google.com/drive/folders/13Hx0NcA66gY6Fl-5L3NjFov0F4KoH36H?usp=sharing*

688 **Figure Legends**

689 ***Figure 1.*** **Physiological adaptations to HIIT**

690 **A**. Experimental overview. **B**. Subject characteristics. **C**. Five weeks of HIIT increased maximal
691 oxygen uptake ($\dot{V}O_{2max}$) and incremental peak power output (iPPO). **D** HIIT increased whole-body
692 fat oxidation during submaximal exercise (50-150 W) without altering **E**. carbohydrate oxidation. **F**.
693 HIIT increased mitochondrial respiration in skeletal muscle (L_N: leak respiration, FAO: fatty acid
694 oxidation, CI_D: submaximal CI respiration, P_D: submaximal CI+II respiration, P: oxidative
695 phosphorylation capacity, E: electron transport system capacity, E_{CII}: succinate-supported electron
696 transport system capacity). **G**. HIIT increased skeletal muscle citrate synthase (CS) activity. **H**.
697 Analytical workflow. Summary statistics are mean ± SEM (n = 8). * $p < 0.05$, ** $p < 0.01$, *** $p <$
698 0.001.

699

700 ***Figure 2.*** **HIIT increases mitochondrial proteins and reduces a subset of contractile fiber**
701 **associated proteins**

702 **A**. Volcano plot displaying 102 upregulated and 24 downregulated proteins following HIIT (FDR <
703 0.05). **B**. Fisher's exact tests identified the enrichment of mitochondrial terms within the differentially
704 regulated proteins (enrichment analysis FDR < 0.02). **C**. Hierarchical clustering and enrichment
705 analysis (enrichment analysis FDR < 0.02) on differentially regulated proteins identified that
706 mitochondrial terms are enriched within the upregulated proteins, while cytoplasm (UniProt
707 Keyword) is enriched amongst the downregulated proteins. **D**. Summed total protein abundances for
708 different organelles (UniProt Keyword) shows upregulation of the mitochondrial protein content. **E-**
709 **G**. Summed total protein abundances display upregulation of electron transport chain complexes (**E**.),
710 mitochondrially-encoded proteins (**F**.) and proteins with a transit peptide (**G**.). Summary statistics are
711 mean ± SEM (n = 8). * $p < 0.05$, ** $p < 0.01$, *** $p < 0.001$.

712

713 ***Figure 3.*** **HIIT regulates proteins involved in skeletal muscle calcium sensitivity and handling**

714 HIIT did not alter the expression of myosin heavy chain (MYH1: MyHC2x, MYH2: MyHC2a,
715 MYH4: MyHC2x, MYH7: MyHCβ; **A**.) or light chain (**B**.) isoforms. **C**. HIIT regulates proteins
716 controlling myosin phosphorylation. **D**. HIIT reduces expression of subunits of the dihydropyridine
717 receptor. **E**. Summed total protein abundances display downregulation of the dihydropyridine
718 receptor. **F**. HIIT does not alter the expression of ryanodine receptor 1. Summary statistics are mean
719 ± SEM (n = 8). ^ FDR < 0.05. * p < 0.05, ** p < 0.01, *** p < 0.001.

720

721 ***Figure 4.*** **The human skeletal muscle acetylome displays higher stoichiometry on mitochondrial**
722 **proteins and lower stoichiometry on contractile proteins**

723 **A**. We quantified 1263 acetyl-sites corresponding to 464 proteins (n = 7). Of these, 421 proteins were
724 also quantified in the proteome with 1232 of the quantified acetyl-sites located on these 421 proteins.
725 **B**. Distribution of acetyl-sites on proteins within the pre-HIIT acetylome. **C**. Top 10 highest intensity
726 acetylated proteins (acetyl-peptide intensities were summed for each protein) within the pre-HIIT
727 acetylome. **D**. Cumulative protein abundance and rank within the proteome (the top 10 highest
728 intensity acetyl-proteins are highlighted). **E**. One-dimensional enrichment analysis of acetylated
729 protein intensity identified mitochondrial proteins, particularly those involved in carboxylic acid
730 metabolism and monovalent inorganic cation transport (e.g. complex V) as having systematically
731 high acetylation intensities (enrichment analysis FDR < 0.02). **F**. Top 10 acetyl-sites with highest
732 abundance-corrected intensities (ACIs). **G**. One-dimensional enrichment analysis of acetyl-site ACIs
733 identified mitochondrial and carboxylic acid catabolic proteins as higher stoichiometry (positive
734 enrichment factor), while contractile fiber cytosolic and plasma membrane proteins were enriched
735 as lower stoichiometry (negative enrichment factor; (enrichment analysis FDR < 0.02; enrichment

736 performed on leading protein IDs). **H**. Histogram depicting the ACI distribution of the total acetylome
737 (blue), the mitochondrial acetyl-sites (green) and the contractile fiber acetyl-sites (yellow).
738 Mitochondrial proteins were distributed at higher ACI values and contractile fiber proteins at lower
739 ACI values than the total acetylome.
740
741 ***Figure 5*. HIIT increases acetylation of mitochondrial and TCA cycle proteins concomitantly**
742 **with an increase in SIRT3 expression**
743 **A**. Volcano plot displaying 20 upregulated (filled red circles) and 1 downregulated (filled blue circle)
744 acetyl-sites following HIIT at an FDR < 0.05, while 257 acetyl-sites were upregulated (red circles)
745 and 26 downregulated (blue circles) at Π < 0.05 (n = 7). **B**. Scatter plot indicating that HIIT-induced
746 changes in acetyl-site intensity typically exceeded that of the corresponding protein. **C**. Fisher's exact
747 tests identified the enrichment of mitochondrial and TCA cycle terms within the differentially
748 regulated acetyl-proteins (enrichment analysis FDR < 0.02; enrichment performed on leading protein
749 IDs). **D**. IceLogo motif enrichment (p < 0.01) for the upregulated sites displayed a predominance of
750 proximal cysteine residues relative to the acetylated lysine (position 0). **E**. Immunoblotting analysis
751 identified the upregulation of SIRT3, but no change in SIRT1, following HIIT (n = 8). * p < 0.05, **
752 p < 0.01, *** p < 0.001.
753
754 ***Figure 6*. Individual acetyl-site regulation of mitochondrial, TCA cycle and contractile proteins**
755 **following HIIT**
756 Regulation of acetyl-sites on **A**. electron transport chain complex subunits (annotated by HUGO), **B**.
757 TCA cycle proteins (annotated by KEGG) and **C**. muscle contraction proteins (annotated by
758 REACTOME).
759

760 ***Figure 7*. HIIT increases acetylation on specific histone acetyl-sites**

761 HIIT increased acetylation on **A**. H1.5 K48, **B**. H2B type 2F K16/20 and **C**. H3 K23. **D**. HIIT did not

762 alter H4 acetylation. Summary statistics are mean ± SEM (n = 7). † Π < 0.05.

763

764 ***Figure S1.* Proteome quality control**

765 **A**. Quantified proteins from each sample. **B**. Representative Pearson correlation between biological

766 replicates (Pre 4 v Pre 5). **C**. Cellular compartment (GOCC) coverage of the proteome.

767

768 ***Figure S2*. HIIT increases electron transport chain subunits**

769 Immunoblotting analyses confirmed the upregulation of electron transport chain proteins. Summary

770 statistics are mean ± SEM (n = 8). * p < 0.05, ** p < 0.01, *** p < 0.001.

771

772 ***Figure S3*. HIIT decreases MYLK2 abundance**

773 **A**. Immunoblotting analysis confirms the downregulation of MYLK2. **B**. No change in the expression

774 of sarcoplasmic/endoplasmic reticulum calcium ATPases 1-3 (SERCAs). Summary statistics are

775 mean ± SEM (n = 8). * p < 0.05, ** p < 0.01, *** p < 0.001.

776

777 ***Figure S4.* Acetylome quality control**

778 **A**. Overlap between identified acetyl-site with those identified in human skeletal muscle by Lundby

779 et al[18]. **B**. Quantified acetyl-sites from each sample. **C**. Representative Pearson correlation between

780 biological replicates (Pre 4 v Pre 5). **D**. Cellular compartment (GOCC) coverage of the acetylome.

781

References

1. Mandsager, K., *et al.* Association of cardiorespiratory fitness with long-term mortality among adults undergoing exercise treadmill testing. *JAMA Network Open* **1**, e183605-e183605 (2018).
2. Deshmukh, A.S., *et al.* Deep muscle-proteomic analysis of freeze-dried human muscle biopsies reveals fiber type-specific adaptations to exercise training. *Nat. Commun.* **12**, 304 (2021).
3. Gonzalez-Franquesa, A., *et al.* Mass-spectrometry based proteomics reveals mitochondrial supercomplexome plasticity. *bioRxiv*, 860080 (2019).
4. Hostrup, M. & Bangsbo, J. Limitations in intense exercise performance of athletes – effect of speed endurance training on ion handling and fatigue development. *J. Physiol.* **595**, 2897-2913 (2017).
5. Egan, B. & Zierath, J.R. Exercise metabolism and the molecular regulation of skeletal muscle adaptation. *Cell. Metab.* **17**, 162-184 (2013).
6. Holloway, K.V., *et al.* Proteomic investigation of changes in human vastus lateralis muscle in response to interval-exercise training. *Proteomics* **9**, 5155-5174 (2009).
7. Robinson, M.M., *et al.* Enhanced protein translation underlies improved metabolic and physical adaptations to different exercise training modes in young and old humans. *Cell. Metab.* **25**, 581-592 (2017).
8. Ubaida-Mohien, C., *et al.* Physical activity associated proteomics of akeletal muscle: Being physically active in daily life may protect skeletal muscle from aging. **10**, 312 (2019).
9. Baeza, J., Smallegan, M.J. & Denu, J.M. Mechanisms and dynamics of protein acetylation in mitochondria. *Trends Biochem. Sci.* **41**, 231-244 (2016).
10. Cohen, P. The regulation of protein function by multisite phosphorylation--a 25 year update. *Trends Biochem. Sci.* **25**, 596-601 (2000).
11. Hoffman, N.J., *et al.* Global phosphoproteomic analysis of human skeletal muscle reveals a network of exercise-regulated kinases and AMPK substrates. *Cell. Metab.* **22**, 922-935 (2015).
12. Overmyer, K.A., *et al.* Maximal oxidative capacity during exercise is associated with skeletal muscle fuel selection and dynamic changes in mitochondrial protein acetylation. *Cell. Metab.* **21**, 468-478 (2015).
13. Parker, B.L., Kiens, B., Wojtaszewski, J.F.P., Richter, E.A. & James, D.E. Quantification of exercise-regulated ubiquitin signaling in human skeletal muscle identifies protein modification cross talk via NEDDylation. *The FASEB Journal* **34**, 5906-5916 (2020).
14. Choudhary, C., Weinert, B.T., Nishida, Y., Verdin, E. & Mann, M. The growing landscape of lysine acetylation links metabolism and cell signalling. *Nature Reviews Molecular Cell Biology* **15**, 536-550 (2014).
15. Hansen, B.K., *et al.* Analysis of human acetylation stoichiometry defines mechanistic constraints on protein regulation. *Nat. Commun.* **10**, 1055 (2019).
16. Narita, T., Weinert, B.T. & Choudhary, C. Functions and mechanisms of non-histone protein acetylation. *Nat. Rev. Mol. Cell Biol.* **20**, 156-174 (2019).
17. Svinkina, T., *et al.* Deep, Quantitative coverage of the lysine acetylome using novel anti-acetyl-lysine antibodies and an optimized proteomic workflow. *Mol. Cell. Proteomics* **14**, 2429-2440 (2015).
18. Lundby, A., *et al.* Proteomic analysis of lysine acetylation sites in rat tissues reveals organ specificity and subcellular patterns. *Cell reports* **2**, 419-431 (2012).
19. Hebert, A.S., *et al.* Calorie restriction and SIRT3 trigger global reprogramming of the mitochondrial protein acetylome. *Mol. Cell* **49**, 186-199 (2013).
20. Pougovkina, O., *et al.* Mitochondrial protein acetylation is driven by acetyl-CoA from fatty acid oxidation. *Hum. Mol. Genet.* **23**, 3513-3522 (2014).
21. Weinert, B.T., Moustafa, T., Iesmantavicius, V., Zechner, R. & Choudhary, C. Analysis of acetylation stoichiometry suggests that SIRT3 repairs nonenzymatic acetylation lesions. *EMBO J.* **34**, 2620-2632 (2015).

22. Williams, A.S., *et al.* Disruption of acetyl-lysine turnover in muscle mitochondria promotes insulin resistance and redox stress without overt respiratory dysfunction. *Cell. Metab.* **31**, 131-147.e111 (2020).
23. Deshmukh, A.S., *et al.* Deep proteomics of mouse skeletal muscle enables quantitation of protein isoforms, metabolic pathways, and transcription factors. *Mol. Cell. Proteomics* **14**, 841-853 (2015).
24. Tabb, D.L., *et al.* Repeatability and reproducibility in proteomic identifications by liquid chromatography-tandem mass spectrometry. *J. Proteome Res.* **9**, 761-776 (2010).
25. Ludwig, C., *et al.* Data-independent acquisition-based SWATH-MS for quantitative proteomics: a tutorial. *Mol. Syst. Biol.* **14**, e8126 (2018).
26. Wen, D., *et al.* Effects of different protocols of high intensity interval training for VO2max improvements in adults: A meta-analysis of randomised controlled trials. *J. Sci. Med. Sport* **22**, 941-947 (2019).
27. Pesta, D., *et al.* Similar qualitative and quantitative changes of mitochondrial respiration following strength and endurance training in normoxia and hypoxia in sedentary humans. *Am. J. Physiol. Regul. Integr. Comp. Physiol.* **301**, R1078-R1087 (2011).
28. Christensen, P.M., *et al.* A short period of high-intensity interval training improves skeletal muscle mitochondrial function and pulmonary oxygen uptake kinetics. *J. Appl. Physiol.* **120**, 1319-1327 (2016).
29. Jacobs, R.A., *et al.* Improvements in exercise performance with high-intensity interval training coincide with an increase in skeletal muscle mitochondrial content and function. *J. Appl. Physiol.* **115**, 785-793 (2013).
30. Dohlmann, T.L., Hindsø, M., Dela, F., Helge, J.W. & Larsen, S. High-intensity interval training changes mitochondrial respiratory capacity differently in adipose tissue and skeletal muscle. *Physiol. Rep.* **6**, e13857 (2018).
31. Granata, C., Oliveira, R.S., Little, J.P., Renner, K. & Bishop, D.J. Training intensity modulates changes in PGC-1alpha and p53 protein content and mitochondrial respiration, but not markers of mitochondrial content in human skeletal muscle. *FASEB J.* **30**, 959-970 (2016).
32. Larsen, S., *et al.* The effect of high-intensity training on mitochondrial fat oxidation in skeletal muscle and subcutaneous adipose tissue. *Scand. J. Med. Sci. Sports* **25**, e59-e69 (2015).
33. Meinild Lundby, A.K., *et al.* Exercise training increases skeletal muscle mitochondrial volume density by enlargement of existing mitochondria and not de novo biogenesis. *Acta physiologica (Oxford, England)* **222**, e12905-n/a (2018).
34. Larsen, S., *et al.* Biomarkers of mitochondrial content in skeletal muscle of healthy young human subjects. *J. Physiol.* **590**, 3349-3360 (2012).
35. Chen, Y., *et al.* GDI-1 preferably interacts with Rab10 in insulin-stimulated GLUT4 translocation. *Biochem. J.* **422**, 229-235 (2009).
36. Wooldridge, A.A., *et al.* Deletion of the protein kinase A/protein kinase G target SMTNL1 promotes an exercise-adapted phenotype in vascular smooth muscle. *The Journal of biological chemistry* **283**, 11850-11859 (2008).
37. Alessi, D., MacDougall, L.K., Sola, M.M., Ikebe, M. & Cohen, P. The control of protein phosphatase-1 by targetting subunits. The major myosin phosphatase in avian smooth muscle is a novel form of protein phosphatase-1. *Eur. J. Biochem.* **210**, 1023-1035 (1992).
38. Davis, J.S., *et al.* The overall pattern of cardiac contraction depends on a spatial gradient of myosin regulatory light chain phosphorylation. *Cell* **107**, 631-641 (2001).
39. Lynch, G.S., McKenna, M.J. & Williams, D.A. Sprint-training effects on some contractile properties of single skinned human muscle fibres. *Acta Physiol. Scand.* **152**, 295-306 (1994).
40. Flucher, B.E. & Franzini-Armstrong, C. Formation of junctions involved in excitation-contraction coupling in skeletal and cardiac muscle. *Proc. Natl. Acad. Sci. U. S. A.* **93**, 8101-8106 (1996).

878 41. Ortenblad, N., Lunde, P.K., Levin, K., Andersen, J.L. & Pedersen, P.K. Enhanced sarcoplasmic reticulum
879 Ca(2+) release following intermittent sprint training. *Am. J. Physiol. Regul. Integr. Comp. Physiol.* **279**,
880 R152-160 (2000).
881 42. Hostrup, M.*, et al.* In-season adaptations to intense intermittent training and sprint interval training
882 in sub-elite football players. *Scand. J. Med. Sci. Sports* **29**, 669-677 (2019).
883 43. Hostrup, M., Onslev, J., Jacobson, G.A., Wilson, R. & Bangsbo, J. Chronic β(2) -adrenoceptor agonist
884 treatment alters muscle proteome and functional adaptations induced by high intensity training in
885 young men. *J. Physiol.* **596**, 231-252 (2018).
886 44. Majerczak, J., Karasinski, J. & Zoladz, J.A. Training induced decrease in oxygen cost of cycling is
887 accompanied by down-regulation of SERCA expression in human vastus lateralis muscle. *J. Physiol.*
888 *Pharmacol.* **59**, 589-602 (2008).
889 45. Munkvik, M.*, et al.* Training effects on skeletal muscle calcium handling in human chronic heart
890 failure. *Med. Sci. Sports Exerc.* **42**, 847-855 (2010).
891 46. Banas, K., Clow, C., Jasmin, B.J. & Renaud, J.M. The KATP channel Kir6.2 subunit content is higher in
892 glycolytic than oxidative skeletal muscle fibers. *Am. J. Physiol. Regul. Integr. Comp. Physiol.* **301**,
893 R916-925 (2011).
894 47. Murgia, M.*, et al.* Single muscle fiber proteomics reveals fiber-type-specific features of human muscle
895 aging. *Cell reports* **19**, 2396-2409 (2017).
896 48. Sterner, D.E. & Berger, S.L. Acetylation of histones and transcription-related factors. *Microbiology*
897 *and molecular biology reviews : MMBR* **64**, 435-459 (2000).
898 49. Strahl, B.D. & Allis, C.D. The language of covalent histone modifications. *Nature* **403**, 41-45 (2000).
899 50. St Clair, D.K., Wan, X.S., Oberley, T.D., Muse, K.E. & St Clair, W.H. Suppression of radiation-induced
900 neoplastic transformation by overexpression of mitochondrial superoxide dismutase. *Mol. Carcinog.*
901 **6**, 238-242 (1992).
902 51. Tao, Z., Gao, P. & Liu, H.W. Identification of the ADP-ribosylation sites in the PARP-1 automodification
903 domain: Analysis and implications. *J. Am. Chem. Soc.* **131**, 14258-14260 (2009).
904 52. Cox, J. & Mann, M. 1D and 2D annotation enrichment: A statistical method integrating quantitative
905 proteomics with complementary high-throughput data. *BMC Bioinformatics* **13 Suppl 16**, S12-S12
906 (2012).
907 53. Freeman, H.C., Hugill, A., Dear, N.T., Ashcroft, F.M. & Cox, R.D. Deletion of Nicotinamide Nucleotide
908 Transhydrogenase. *Diabetes* **55**, 2153 (2006).
909 54. Ho, H.-Y., Lin, Y.-T., Lin, G., Wu, P.-R. & Cheng, M.-L. Nicotinamide nucleotide transhydrogenase
910 (NNT) deficiency dysregulates mitochondrial retrograde signaling and impedes proliferation. *Redox*
911 *Biology* **12**, 916-928 (2017).
912 55. Foster, D.B.*, et al.* The Cardiac Acetyl-Lysine Proteome. *PLoS One* **8**, e67513 (2013).
913 56. Tyanova, S.*, et al.* The Perseus computational platform for comprehensive analysis of (prote)omics
914 data. *Nature Methods* **13**, 731 (2016).
915 57. Weinert, B.T.*, et al.* Acetylation dynamics and stoichiometry in Saccharomyces cerevisiae. *Mol. Syst.*
916 *Biol.* **10**, 716 (2014).
917 58. Pietrocola, F., Galluzzi, L., Bravo-San Pedro, José M., Madeo, F. & Kroemer, G. Acetyl coenzyme A: A
918 central metabolite and second messenger. *Cell. Metab.* **21**, 805-821 (2015).
919 59. Xiao, Y.*, et al.* A novel significance score for gene selection and ranking. *Bioinformatics* **30**, 801-807
920 (2014).
921 60. Colaert, N., Helsens, K., Martens, L., Vandekerckhove, J. & Gevaert, K. Improved visualization of
922 protein consensus sequences by iceLogo. *Nat Methods* **6**, 786-787 (2009).
923 61. James, A.M., Smith, A.C., Smith, C.L., Robinson, A.J. & Murphy, M.P. Proximal Ccsteines that enhance
924 lysine N-acetylation of cytosolic proteins in mice are less conserved in longer-living species. *Cell*
925 *reports* **24**, 1445-1455 (2018).
926 62. Putman, C.T.*, et al.* Effects of short-term submaximal training in humans on muscle metabolism in
927 exercise. *Am J Physiol Endocrinol Metab* **275**, E132-E139 (1998).

63. Constantin-Teodosiu, D., Carlin, J.I., Cederblad, G., Harrist, R.C. & Hultman, E. Acetyl group accumulation and pyruvate dehydrogenase activity in human muscle during incremental exercise. *Acta Physiol. Scand.* **143**, 367-372 (1991).
64. Gibala, M.J., MacLean, D.A., Graham, T.E. & Saltin, B. Tricarboxylic acid cycle intermediate pool size and estimated cycle flux in human muscle during exercise. *Am. J. Physiol.* **275**, E235-242 (1998).
65. Howlett, R.A.*, et al.* Regulation of skeletal muscle glycogen phosphorylase and PDH at varying exercise power outputs. *Am. J. Physiol.* **275**, R418-425 (1998).
66. Hirschey, M.D.*, et al.* SIRT3 regulates mitochondrial fatty-acid oxidation by reversible enzyme deacetylation. *Nature* **464**, 121-125 (2010).
67. Tao, R.*, et al.* Sirt3-mediated deacetylation of evolutionarily conserved lysine 122 regulates MnSOD activity in response to stress. *Mol. Cell* **40**, 893-904 (2010).
68. Vassilopoulos, A.*, et al.* SIRT3 deacetylates ATP synthase F1 complex proteins in response to nutrient- and exercise-induced stress. *Antioxid. Redox. Signal.* **21**, 551-564 (2014).
69. Braschi, B.*, et al.* Genenames.org: the HGNC and VGNC resources in 2019. *Nucleic Acids Res.* **47**, D786-D792 (2019).
70. Campanella, M.*, et al.* Regulation of mitochondrial structure and function by the F1Fo-ATPase inhibitor protein, IF1. *Cell. Metab.* **8**, 13-25 (2008).
71. Hendzel, M.J., Sun, J.M., Chen, H.Y., Rattner, J.B. & Davie, J.R. Histone acetyltransferase is associated with the nuclear matrix. **269**, 22894-22901 (1994).
72. Joseph, J.S., Ayeleso, A.O. & Mukwevho, E. Exercise increases hyper-acetylation of histones on the Cis-element of NRF-1 binding to the Mef2a promoter: Implications on type 2 diabetes. *Biochem. Biophys. Res. Commun.* **486**, 83-87 (2017).
73. Lochmann, T.L., Thomas, R.R., Bennett, J.P., Jr. & Taylor, S.M. Epigenetic modifications of the PGC-1α promoter during exercise induced expression in mice. *PLoS One* **10**, e0129647 (2015).
74. McGee, S.L., Fairlie, E., Garnham, A.P. & Hargreaves, M. Exercise-induced histone modifications in human skeletal muscle. *J. Physiol.* **587**, 5951-5958 (2009).
75. Smith, J.A., Kohn, T.A., Chetty, A.K. & Ojuka, E.O. CaMK activation during exercise is required for histone hyperacetylation and MEF2A binding at the MEF2 site on the Glut4 gene. *Am J Physiol Endocrinol Metab* **295**, E698-704 (2008).
76. Chen, H.*, et al.* MacroH2A1.1 and PARP-1 cooperate to regulate transcription by promoting CBP-mediated H2B acetylation. *Nat. Struct. Mol. Biol.* **21**, 981-989 (2014).
77. Parra, M.A., Kerr, D., Fahy, D., Pouchnik, D.J. & Wyrick, J.J. Deciphering the roles of the histone H2B N-terminal domain in genome-wide transcription. *Mol. Cell. Biol.* **26**, 3842-3852 (2006).
78. Lv, D.*, et al.* Histone acetyltransferase KAT6A upregulates PI3K/AKT Ssgnaling through TRIM24 binding. *Cancer Res.* **77**, 6190-6201 (2017).
79. Tsai, W.-W.*, et al.* TRIM24 links a non-canonical histone signature to breast cancer. *Nature* **468**, 927-932 (2010).
80. Pathiraja, T.N.*, et al.* TRIM24 links glucose metabolism with transformation of human mammary epithelial cells. *Oncogene* **34**, 2836-2845 (2015).
81. Ribas, V.*, et al.* Skeletal muscle action of estrogen receptor α is critical for the maintenance of mitochondrial function and metabolic homeostasis in females. *Sci. Transl. Med.* **8**, 334ra354 (2016).
82. Nana, A., Slater, G.J., Hopkins, W.G. & Burke, L.M. Effects of daily activities on dual-energy X-ray absorptiometry measurements of body composition in active people. *Med. Sci. Sports Exerc.* **44**, 180-189 (2012).
83. Berg, H.E., Tedner, B. & Tesch, P.A. Changes in lower limb muscle cross-sectional area and tissue fluid volume after transition from standing to supine. *Acta Physiol. Scand.* **148**, 379-385 (1993).
84. Cerniglia, L.M., Delmonico, M.J., Lindle, R., Hurley, B.F. & Rogers, M.A. Effects of acute supine rest on mid-thigh cross-sectional area as measured by computed tomography. *Clin. Physiol. Funct. Imaging* **27**, 249-253 (2007).

977 85. Jeukendrup, A.E. & Wallis, G.A. Measurement of substrate oxidation during exercise by means of gas
978 exchange measurements. *Int. J. Sports Med.* **26 Suppl 1**, S28-37 (2005).
979 86. Lee, P., Day, R.O., Greenfield, J.R. & Ho, K.K. Formoterol, a highly β2-selective agonist, increases
980 energy expenditure and fat utilisation in men. *Int. J. Obes. (Lond.)* **37**, 593-597 (2013).
981 87. Pesta, D. & Gnaiger, E. High-resolution respirometry: OXPHOS protocols for human cells and
982 permeabilized fibers from small biopsies of human muscle. *Methods Mol. Biol.* **810**, 25-58 (2012).
983 88. Lowry, O. *A flexible system of enzymatic analysis*, (Elsevier, 2012).
984 89. Rappsilber, J., Mann, M. & Ishihama, Y. Protocol for micro-purification, enrichment, pre-fractionation
985 and storage of peptides for proteomics using StageTips. *Nat. Protoc.* **2**, 1896-1906 (2007).
986 90. Kulak, N.A., Geyer, P.E. & Mann, M. Loss-less nano-fractionator for high sensitivity, high coverage
987 proteomics. *Mol. Cell. Proteomics* **16**, 694-705 (2017).
988 91. Cox, J. & Mann, M. MaxQuant enables high peptide identification rates, individualized p.p.b.-range
989 mass accuracies and proteome-wide protein quantification. *Nat. Biotechnol.* **26**, 1367-1372 (2008).
990 92. Bruderer, R.*, et al.* Extending the limits of quantitative proteome profiling with data-independent
991 acquisition and application to acetaminophen-treated three-dimensional liver microtissues. *Mol.*
992 *Cell. Proteomics* **14**, 1400-1410 (2015).
993 93. Wisniewski, J.R. Label-Free and standard-free absolute quantitative proteomics using the "Total
994 Protein" and "Proteomic Ruler" approaches. *Methods Enzymol.* **585**, 49-60 (2017).
995 94. Szklarczyk, D.*, et al.* STRING v11: protein-protein association networks with increased coverage,
996 supporting functional discovery in genome-wide experimental datasets. *Nucleic Acids Res.* **47**, D607-
997 d613 (2019).

Figure 1

A

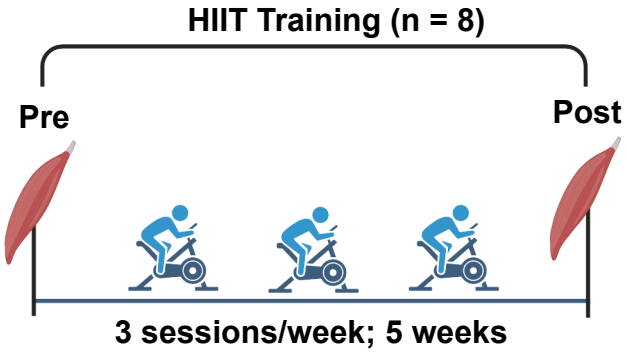

B

Subject characteristics

	Pre	Post
Age (years)	27 ± 2	
Height (cm)	187 ± 2	
Weight (kg)	82.2 ± 3.7	81.8 ± 3.4
BMI (kg·m^{-2})	23.5 ± 0.9	23.4 ± 0.8
Lean mass (kg)	59.1 ± 1.2	60.1 ± 1.2**
Fat mass (kg)	19.7 ± 2.9	18.9 ± 2.6
$\dot{V}O_2$max (mL·min^{-1})	3669 ± 334	4200 ± 117***
$\dot{V}O_2$max (mL·kg^{-1}·min^{-1})	45.3 ± 6.9	51.8 ± 1.9***
iPPO (W)	340 ± 18	400 ± 13***

C

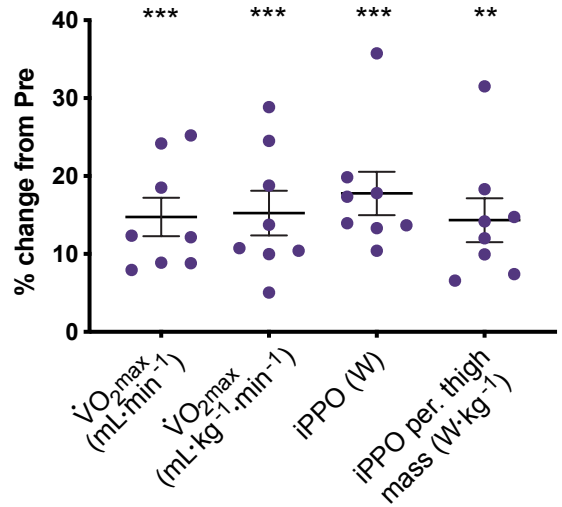

D

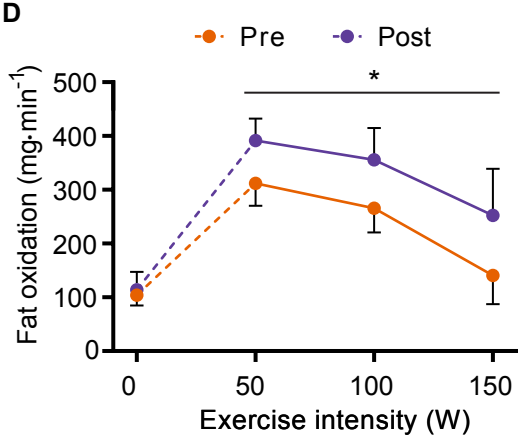

E

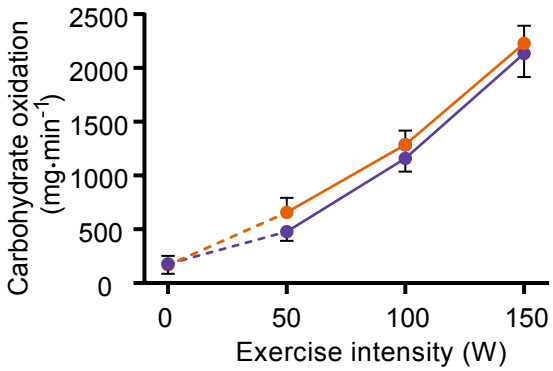

F

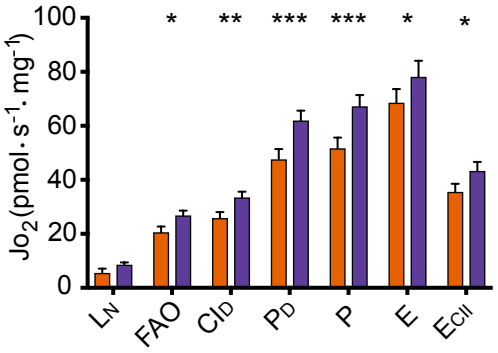

G

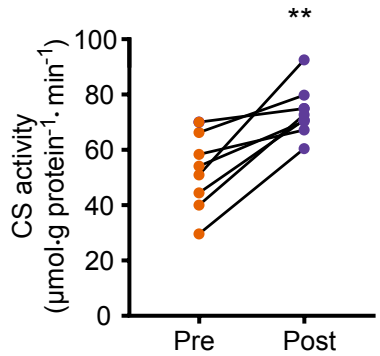

H

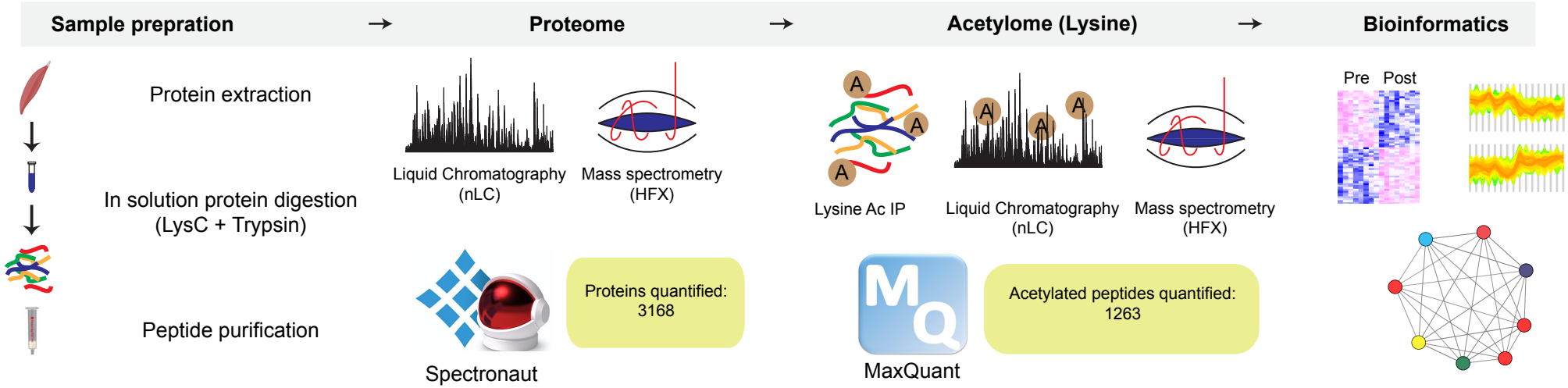

Figure 2

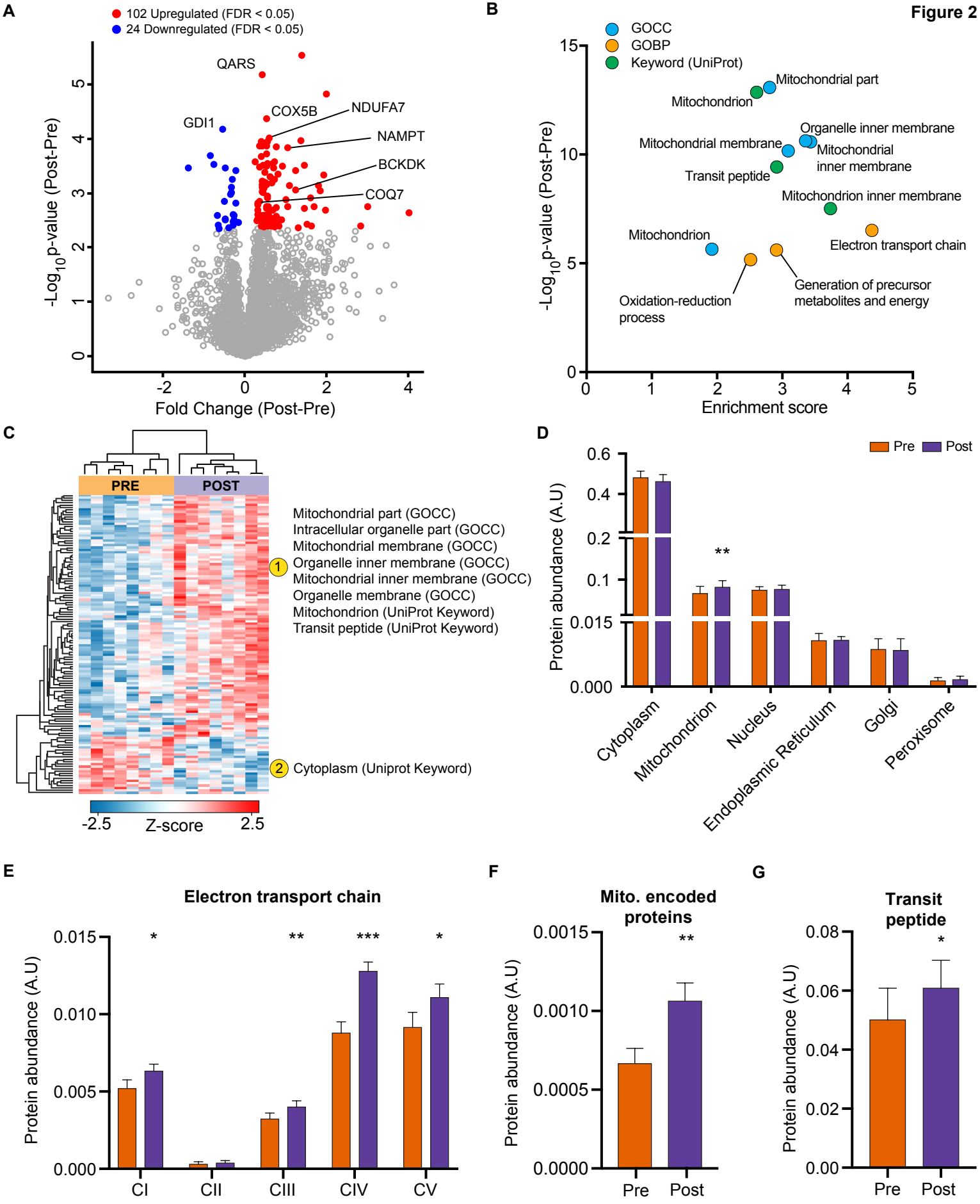
A
102 Upregulated (FDR < 0.05)
24 Downregulated (FDR < 0.05)
QARS
COX5B
NDUFA7
GDI1
NAMPT
BCKDK
COQ7
-Log10 p-value (Post-Pre)
Fold Change (Post-Pre)
B
GOCC
GOBP
Keyword (UniProt)
Mitochondrial part
Mitochondrion
Organelle inner membrane
Mitochondrial membrane
Mitochondrial inner membrane
Transit peptide
Mitochondrion inner membrane
Electron transport chain
Mitochondrion
Generation of precursor metabolites and energy
Oxidation-reduction process
-Log10 p-value (Post-Pre)
Enrichment score
C
PRE
POST
Mitochondrial part (GOCC)
Intracellular organelle part (GOCC)
Mitochondrial membrane (GOCC)
1 Organelle inner membrane (GOCC)
Mitochondrial inner membrane (GOCC)
Organelle membrane (GOCC)
Mitochondrion (UniProt Keyword)
Transit peptide (UniProt Keyword)
2 Cytoplasm (Uniprot Keyword)
-2.5
Z-score
2.5
D
Pre
Post
Protein abundance (A.U)
Cytoplasm
Mitochondrion
Nucleus
Endoplasmic Reticulum
Golgi
Peroxisome
E
Electron transport chain
Protein abundance (A.U)
CI
CII
CIII
CIV
CV
F
Mito. encoded proteins
Protein abundance (A.U)
Pre
Post
G
Transit peptide
Protein abundance (A.U)
Pre
Post

Figure 3

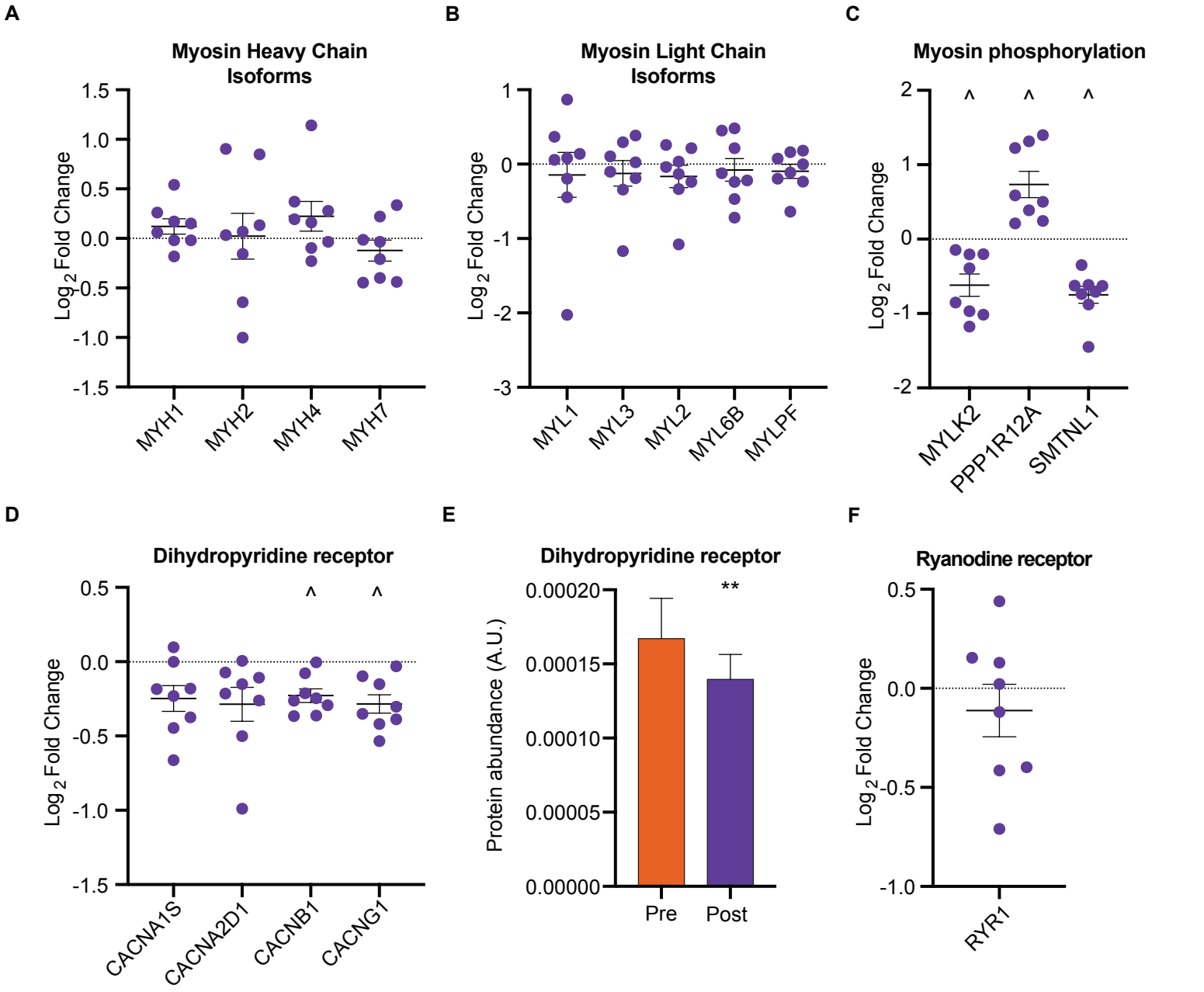
A
Myosin Heavy Chain Isoforms
Log2 Fold Change
1.5
1.0
0.5
0.0
-0.5
-1.0
-1.5
MYH1
MYH2
MYH4
MYH7
B
Myosin Light Chain Isoforms
Log2 Fold Change
1
0
-1
-2
-3
MYL1
MYL3
MYL2
MYL6B
MYLPF
C
Myosin phosphorylation
Log2 Fold Change
2
1
0
-1
-2
^
^
^
MYLK2
PPP1R12A
SMTNL1
D
Dihydropyridine receptor
Log2 Fold Change
0.5
0.0
-0.5
-1.0
-1.5
^
^
CACNA1S
CACNA2D1
CACNB1
CACNG1
E
Dihydropyridine receptor
Protein abundance (A.U.)
0.00020
0.00015
0.00010
0.00005
0.00000
**
Pre
Post
F
Ryanodine receptor
Log2 Fold Change
0.5
0.0
-0.5
-1.0
RYR1

Figure 4

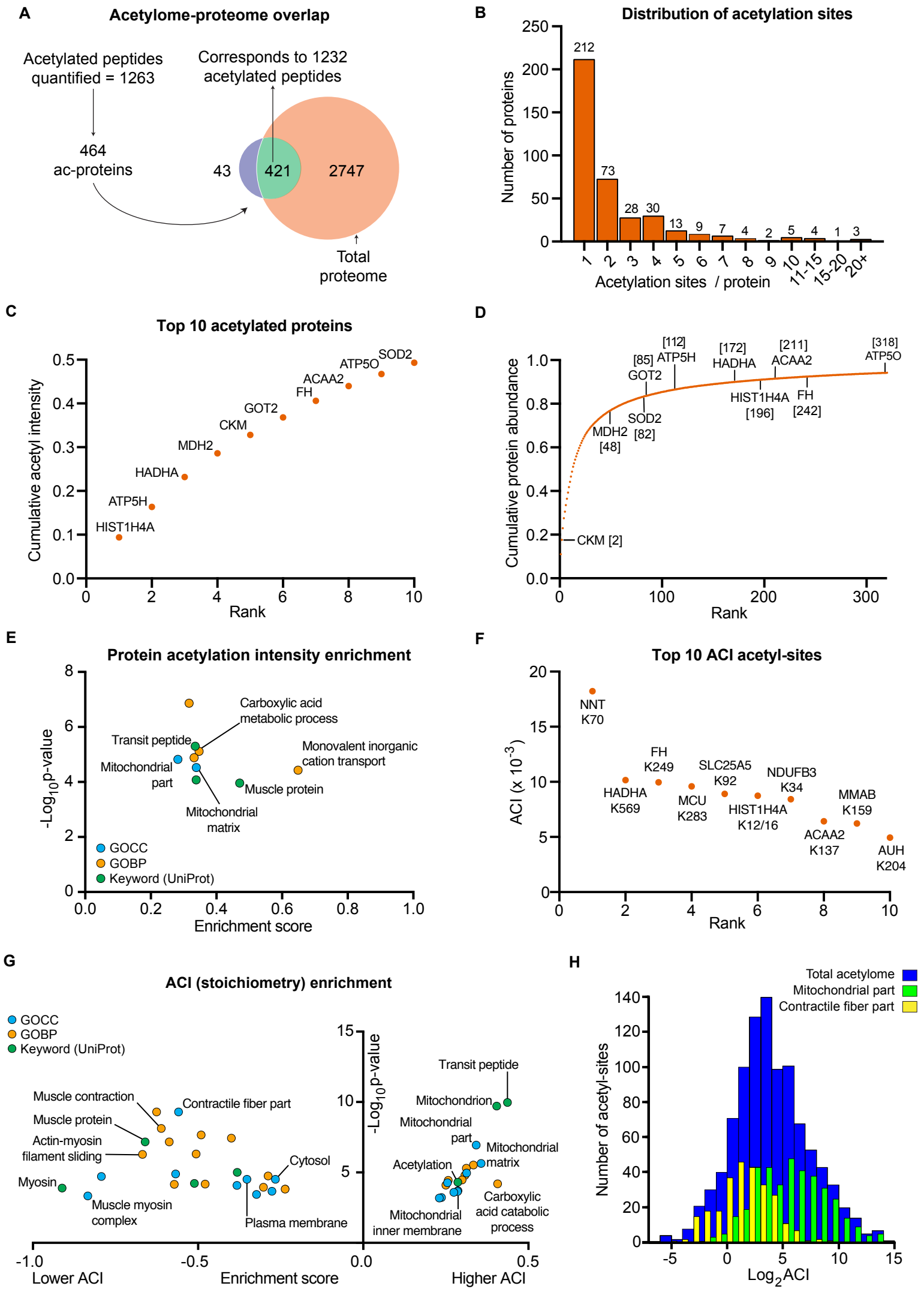
A
Acetylome-proteome overlap
Acetylated peptides quantified = 1263
464 ac-proteins
Corresponds to 1232 acetylated peptides
43
421
2747
Total proteome
B
Distribution of acetylation sites
Number of proteins
Acetylation sites / protein
212
73
28
30
13
9
7
4
2
5
4
1
3
1
2
3
4
5
6
7
8
9
10
11-15
15-20
20+
C
Top 10 acetylated proteins
Cumulative acetyl intensity
Rank
SOD2
ATP5O
ACAA2
FH
GOT2
CKM
MDH2
HADHA
ATP5H
HIST1H4A
D
Cumulative protein abundance
Rank
[318] ATP5O
[211] ACAA2
[172] HADHA
[112] ATP5H
[85] GOT2
HIST1H4A [196]
FH [242]
SOD2 [82]
MDH2 [48]
CKM [2]
E
Protein acetylation intensity enrichment
-Log10p-value
Enrichment score
Carboxylic acid metabolic process
Transit peptide
Monovalent inorganic cation transport
Mitochondrial part
Muscle protein
Mitochondrial matrix
GOCC
GOBP
Keyword (UniProt)
F
Top 10 ACI acetyl-sites
ACI (x 10-3)
Rank
NNT K70
FH K249
SLC25A5 K92
NDUFB3 K34
HADHA K569
MCU K283
HIST1H4A K12/16
MMAB K159
ACAA2 K137
AUH K204
G
ACI (stoichiometry) enrichment
GOCC
GOBP
Keyword (UniProt)
-Log10p-value
Muscle contraction
Contractile fiber part
Muscle protein
Actin-myosin filament sliding
Myosin
Muscle myosin complex
Cytosol
Plasma membrane
Transit peptide
Mitochondrion
Mitochondrial part
Mitochondrial matrix
Acetylation
Carboxylic acid catabolic process
Mitochondrial inner membrane
Lower ACI
Enrichment score
Higher ACI
H
Total acetylome
Mitochondrial part
Contractile fiber part
Number of acetyl-sites
Log2ACI

Figure 5

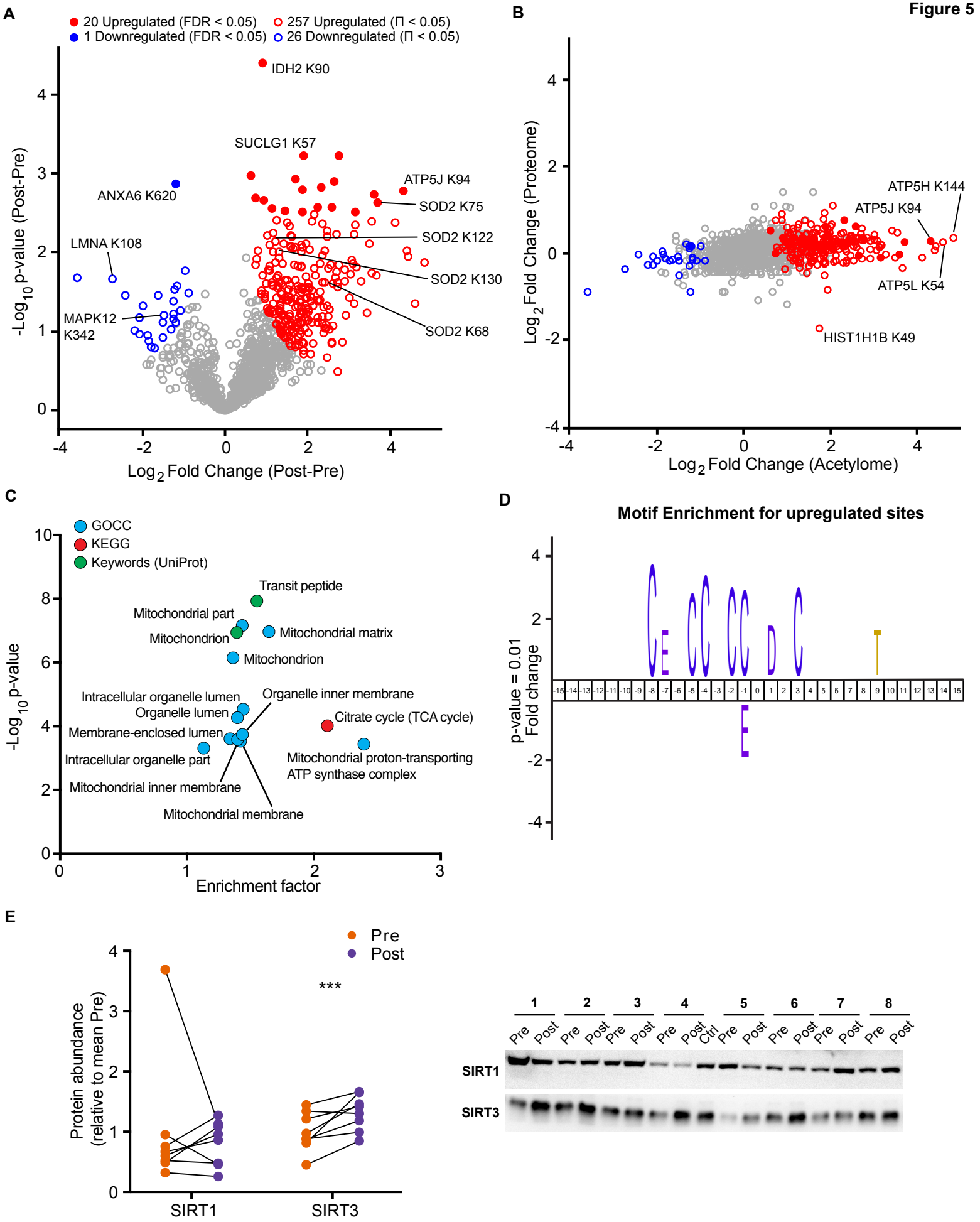
A
20 Upregulated (FDR < 0.05)
257 Upregulated (Π < 0.05)
1 Downregulated (FDR < 0.05)
26 Downregulated (Π < 0.05)
IDH2 K90
SUCLG1 K57
ATP5J K94
SOD2 K75
SOD2 K122
SOD2 K130
SOD2 K68
ANXA6 K620
LMNA K108
MAPK12 K342
-Log10 p-value (Post-Pre)
Log2 Fold Change (Post-Pre)
B
ATP5H K144
ATP5J K94
ATP5L K54
HIST1H1B K49
Log2 Fold Change (Proteome)
Log2 Fold Change (Acetylome)
C
GOCC
KEGG
Keywords (UniProt)
Transit peptide
Mitochondrial part
Mitochondrion
Mitochondrial matrix
Mitochondrion
Intracellular organelle lumen
Organelle lumen
Organelle inner membrane
Citrate cycle (TCA cycle)
Membrane-enclosed lumen
Intracellular organelle part
Mitochondrial proton-transporting ATP synthase complex
Mitochondrial inner membrane
Mitochondrial membrane
-Log10 p-value
Enrichment factor
D
Motif Enrichment for upregulated sites
p-value = 0.01
Fold change
E
Pre
Post
***
Protein abundance (relative to mean Pre)
SIRT1
SIRT3
1
2
3
4
5
6
7
8
Pre
Post
Ctrl
SIRT1
SIRT3

Figure 6

A

Protein:

Log$_2$ fold change (protein)

-2 2

Undetected

Acetylation site:

- Upregulated (Π < 0.05)
- Downregulated (Π < 0.05)
- Unchanged (Π > 0.05)

NDUFAB1, NDUFA9, NDUFA10, NDUFV1, NDUFA2, NDUFV2, NDUFB9, NDUFV3, NDUFA7, NDUFB6, NDUFS5, NDUFS6, NDUFS1, NDUFA5, NDUFB3

SDHA, SDHB

MT-ATP8, ATP5H, ATP5B, ATP5O, ATP5C1, ATP5J, ATP5D, ATP5L, ATP5F1, ATP5A1, ATPIF1, ATP5E

CI, CII, CIII, CIV, CV

UQCRC2, CYC1, UQCRB, UQCRH, UQCRC1

COX4I1, COX6B1, COX5B

B

Pyruvate

PDHX, PDHA1, DLAT

Acetyl CoA

CS

Oxaloacetate

Citrate

ACO2

MDH1, MDH2

Malate

Isocitrate

IDH3A, IDH1, IDH3B, IDH2

FH

TCA Cycle

Fumarate

2-oxogluterate

SDHA, SDHB

OGDH, DLST

Succinate

SUCLG2, SUCLG1, DLD

Succinyl CoA

SUCLA2

C

ACTC1, MYH4, MYBPC1, ACTN2

MYL1, MYH3, MYL2, TNNT1, TNNI1

MYH7, MYH9, TPM2, NEB

ACTN3, DMD, MYH1, TTN

TPM4

VIM

TNNT3, TNNI2, MYL3, DES

MYH2, TPM1, TPM3, MYBPC2

Figure 7

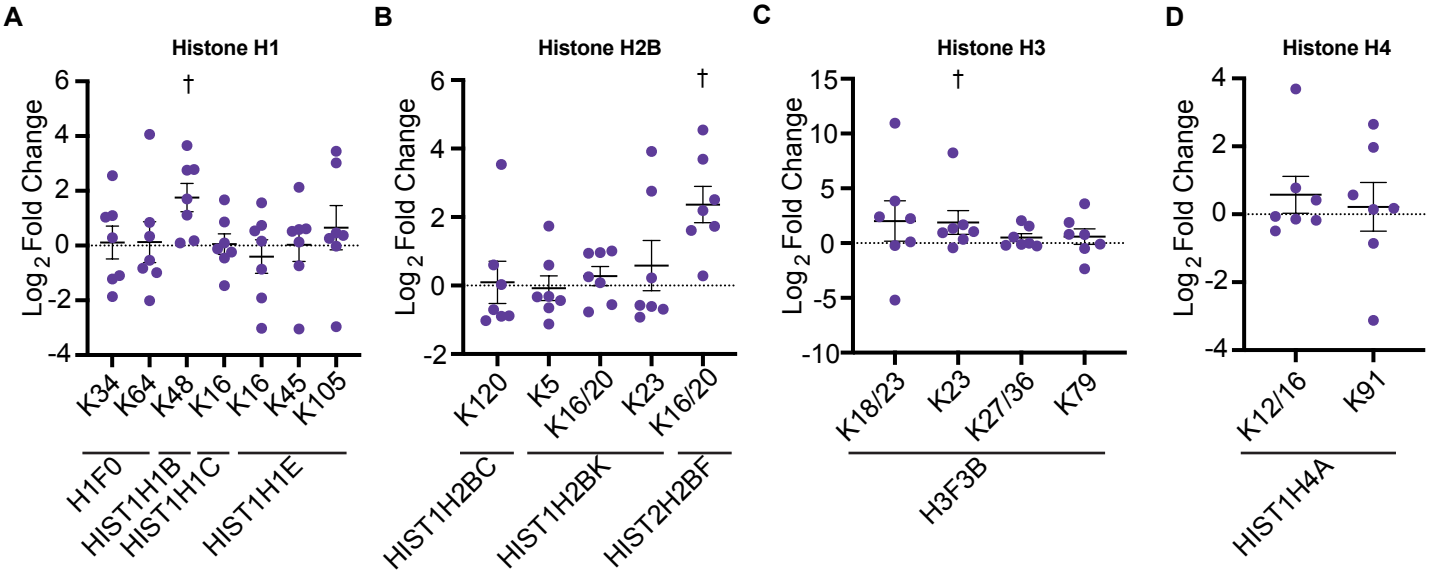
A
Histone H1
Log2 Fold Change
6
4
2
0
-2
-4
†
K34
K64
K48
K16
K16
K45
K105
H1F0
HIST1H1B
HIST1H1C
HIST1H1E
B
Histone H2B
Log2 Fold Change
6
4
2
0
-2
†
K120
K5
K16/20
K23
K16/20
HIST1H2BC
HIST1H2BK
HIST2H2BF
C
Histone H3
Log2 Fold Change
15
10
5
0
-5
-10
†
K18/23
K23
K27/36
K79
H3F3B
D
Histone H4
Log2 Fold Change
4
2
0
-2
-4
K12/16
K91
HIST1H4A

Figure S1

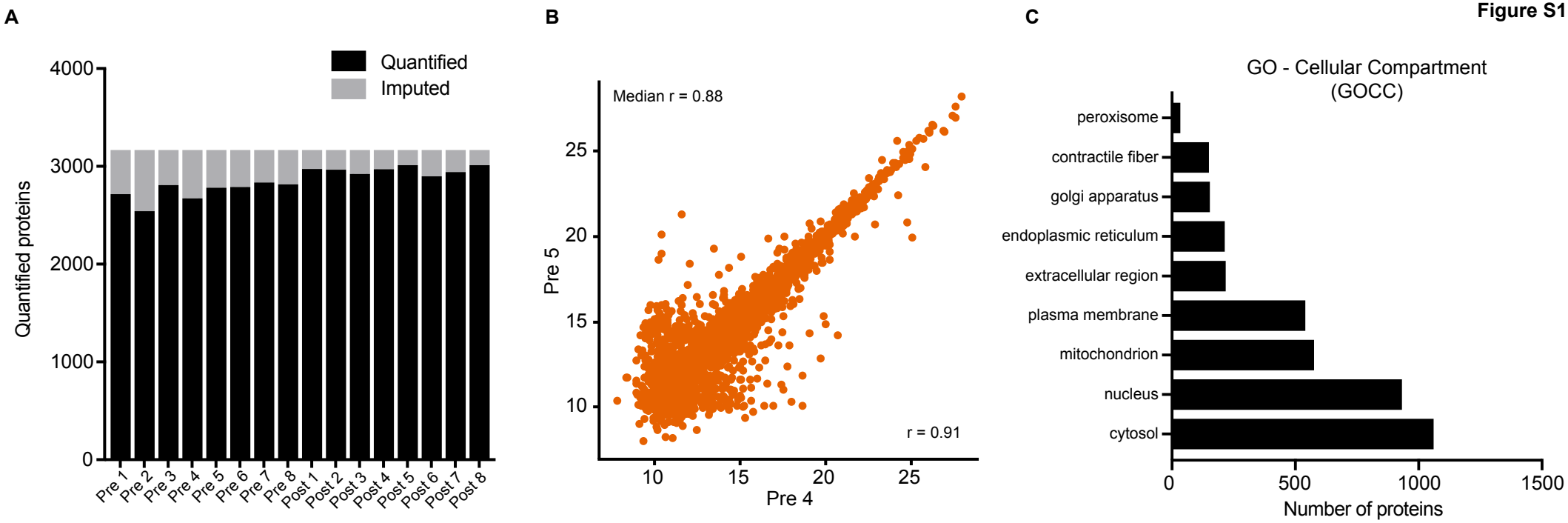
A
Quantified
Imputed
Quantified proteins
4000
3000
2000
1000
0
Pre 1
Pre 2
Pre 3
Pre 4
Pre 5
Pre 6
Pre 7
Pre 8
Post 1
Post 2
Post 3
Post 4
Post 5
Post 6
Post 7
Post 8
B
Median r = 0.88
r = 0.91
Pre 5
Pre 4
10
15
20
25
C
GO - Cellular Compartment
(GOCC)
peroxisome
contractile fiber
golgi apparatus
endoplasmic reticulum
extracellular region
plasma membrane
mitochondrion
nucleus
cytosol
0
500
1000
1500
Number of proteins

Figure S2

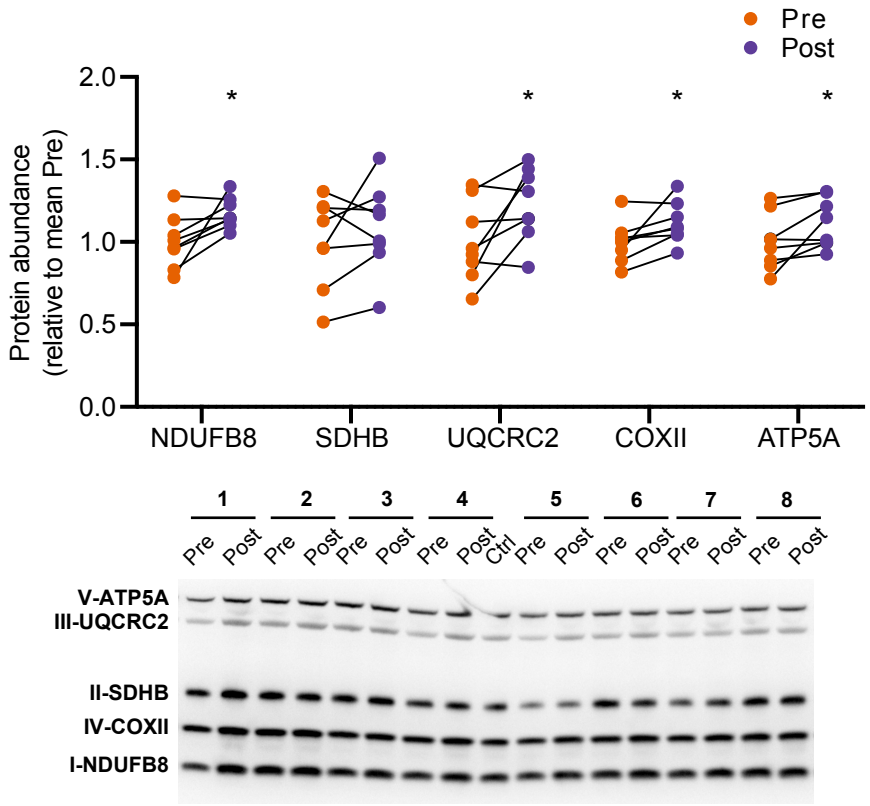
Pre
Post
Protein abundance
(relative to mean Pre)
2.0
1.5
1.0
0.5
0.0
*
*
*
*
NDUFB8
SDHB
UQCRC2
COXII
ATP5A
1
2
3
4
5
6
7
8
Pre
Post
Pre
Post
Pre
Post
Pre
Post
Ctrl
Pre
Post
Pre
Post
Pre
Post
Pre
Post
V-ATP5A
III-UQCRC2
II-SDHB
IV-COXII
I-NDUFB8

Figure S3

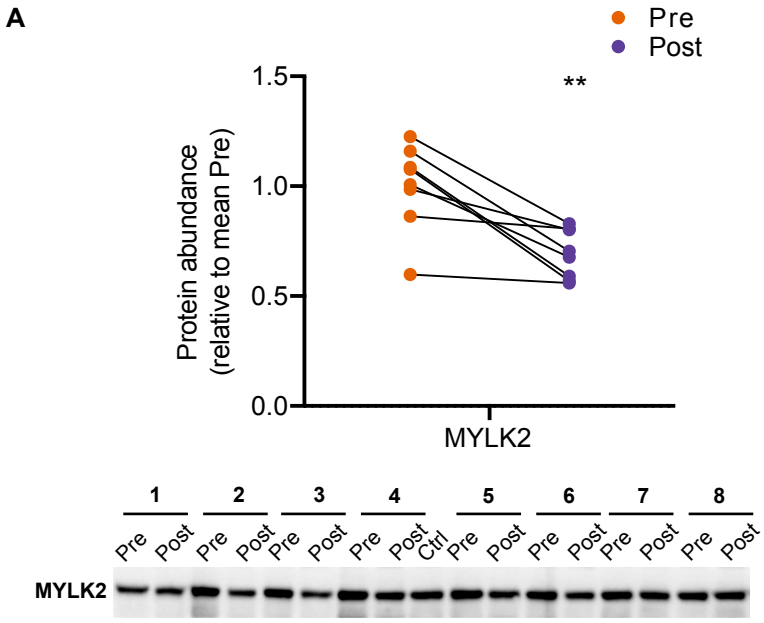
A
Pre
Post
Protein abundance
(relative to mean Pre)
1.5
1.0
0.5
0.0
**
MYLK2
1
2
3
4
5
6
7
8
Pre
Post
Ctrl
MYLK2

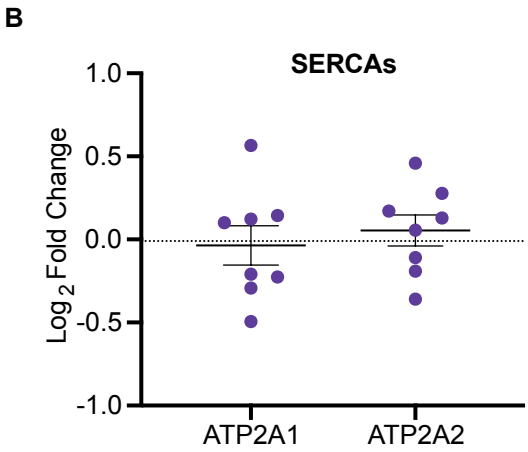
B
SERCAs
Log 2 Fold Change
1.0
0.5
0.0
-0.5
-1.0
ATP2A1
ATP2A2

Figure S4

A

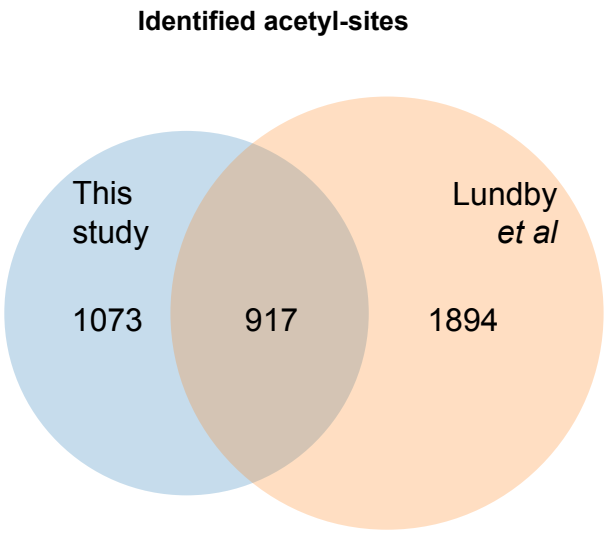

B

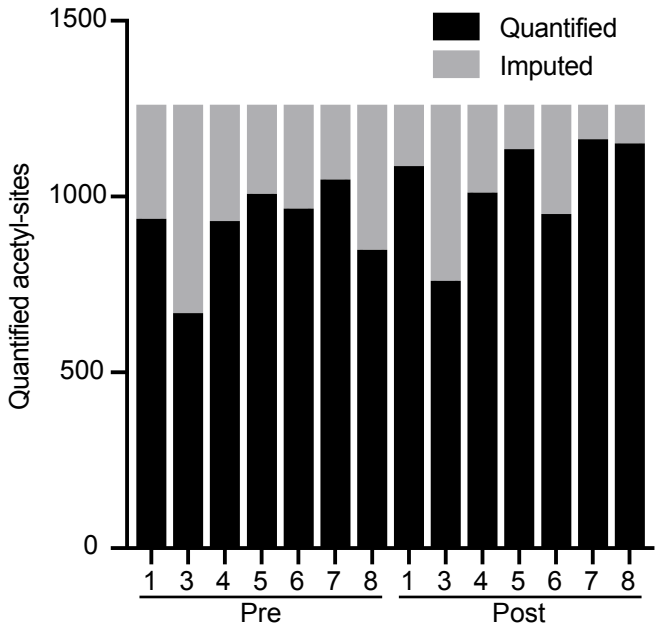

C

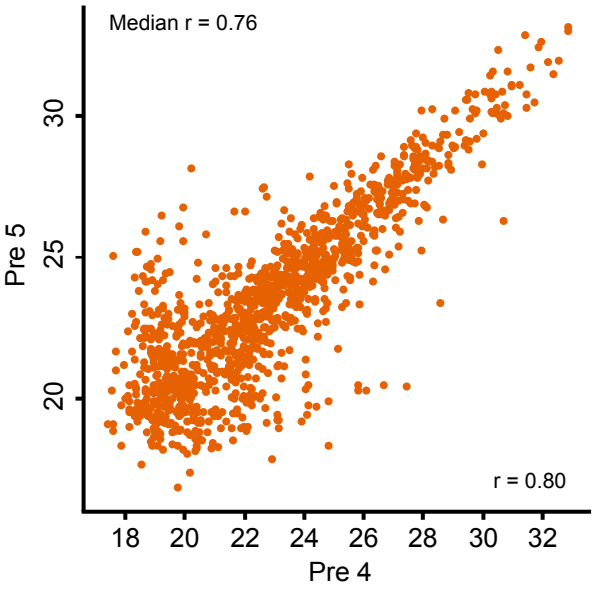
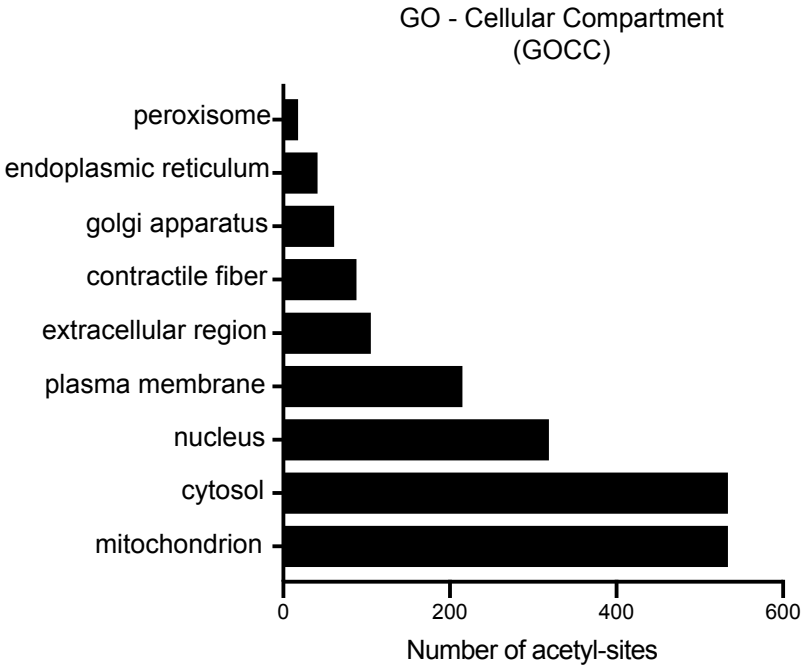
D